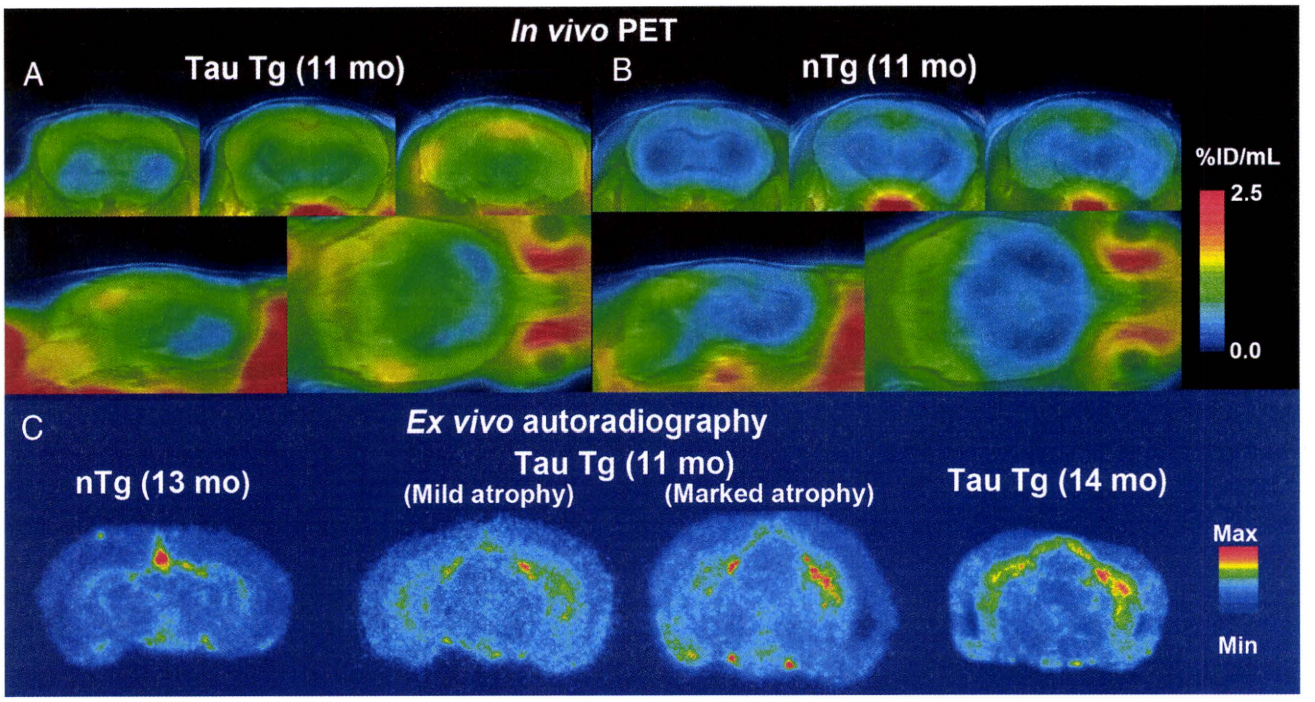

Figure 2. ***A–C***, Induction of neuroinflammatory TSPO signals in PS19 mice detected by *in vivo* PET (***A***, ***B***) and *ex vivo* autoradiographic (***C***) imaging with [^{11}C]AC-5216. ***A***, ***B***, Orthogonal views of TSPO distributions in brains of 11-month-old nTg (***A***) and PS19 Tg (***B***) mice scanned by PET at 30–90 min after intravenous injection of [^{11}C]AC-5216. Coronal images (top) were generated to include the striatum (left; bregma +0.5 mm) and dorsal (middle; bregma −2.2 mm) and ventral (right; bregma −3.6 mm) hippocampi, and sagittal (bottom left) and horizontal (bottom right) slices were constructed at 1.7 mm lateral to the midline and 3.0 mm ventral to the bregma, respectively. PET maps are superimposed on the MRI anatomical template. ***C***, *Ex vivo* autoradiographic mapping of TSPO in brains of 13-month-old nTg mouse, 11-month-old PS19 mouse with marginal neurodegenerative changes, and 11- and 14-month-old PS19 mice with massive neuronal loss in the hippocampus and entorhinal cortex. Brain tissues were collected at 30 min after intravenous injection of [^{11}C]AC-5216, and coronal sections were generated to contain the hippocampus (bregma −2.8 mm).

Bonferroni's test) (Fig. 5*B*). In view of a known finding that PS19 mice exhibit MRI-detectable hippocampal atrophy from 9 months of age (Yoshiyama et al., 2007), this result indicates that TSPO elevates antecedent to measurable neuronal loss at an *in vivo* level. Age-related intensification of TSPO signals in the hippocampus of PS19 mice was also supported by the scatterplot of BP_{ND} for [^{11}C]AC-5216 against age (Fig. 5*C*), with these two parameters showing a significant correlation with each other ($r^2 = 0.40$, $p < 0.001$ by Pearson's correlation coefficient). Notably, a longitudinal series of PET scans of hippocampal BP_{ND} in nine PS19 mice revealed that progression of TSPO upregulation is individually assessable (Fig. 5*C*, red symbols). Notwithstanding the statistical significance of its correlation with age, hippocampal BP_{ND} values displayed a large variance among individuals at the same age (Fig. 5*C*), and thus the level of TSPO expression in each PS19 mouse was not simply predictable by its age.

Next, we sought a neuropathological determinant of TSPO radiosignals by combined autoradiographic and histological assays using sliced brains of PS19 mice aged 3–17 months. In hippocampal sections displaying intense *in vitro* binding of [^{11}C]AC-5216, phosphorylated tau immunoreactivity was markedly enhanced, while no or only several NFT-like amyloid inclusions were detected by thioflavin-S staining (Fig. 5*D–F*). Radiolabeling of TSPO with [^{11}C]AC-5216 was linearly proportional to the amount of phospho-tau immunolabeling (Fig. 5*G*), and an excellent correlation between these two measures was observed according to partial correlation analysis ($r^2 = 0.95$, $p < 0.001$). Radiotracer binding also showed a tendency to correlate with age (Fig. 5*H*), but the partial correlation was not statistically significant in these test samples ($r^2 = 0.32$, $p > 0.05$). Hence, deposition of pathologically phosphorylated tau proteins rather than thioflavin-S-positive high-order tau assembly was the primary determinant of the increase in [^{11}C]AC-5216-labeled TSPO, and interindividual variability in the onset and chronological rate of tau pathogenesis largely modified the course of neuroinflammatory changes during aging.

In vivo imaging of glial response to amyloid accumulation in APP23 mouse brains assessed by [^{11}C]AC-5216 and [^{11}C]PIB

Spatial mapping of [^{11}C]AC-5216 retention in brains of 24-month-old nTg and APP23 mice illustrated the glial response to amyloid deposition in the neocortex and hippocampus (Fig. 6*A*). This observation was also supported by *ex vivo* (Fig. 6*B*) and *in vitro* (Fig. 6*C*) autoradiograms using [^{11}C]AC-5216, and radiolabeling of TSPO was well colocalized with subsequent FSB staining of amyloid plaques in these regions (Fig. 6*C*). In accordance with our previous report (Ji et al., 2008), TSPO immunoreactivity was present primarily in astrocytes surrounding plaques (data not shown).

Time-radioactivity curves generated from dynamic [^{11}C]AC-5216-PET data indicated lower levels of initial radiotracer uptake in all examined regions of APP23 mice ($n = 9$) than in nTg controls ($n = 5$) (Fig. 7*A–C*). Despite this difference, Tg mice exhibited augmented radioactivity retention relative to control mice in the hippocampus and neocortex beyond 45 min after tracer injection (Fig. 7*A*,*B*). Unlike these areas, radiosignals in the striatum of Tg mice beyond 60 min were nearly equivalent to those of controls (Fig. 7*C*), justifying the use of striatal data as reference. Indeed, the ratios of radioactivities to striatal values were significantly increased in the hippocampus (Fig. 7*D*) ($F_{(1,12)} = 5.3$, $p < 0.05$ for main effect of genotype) and neocortex (Fig. 7*E*) ($F_{(1,12)} = 8.0$, $p < 0.05$ for main effect of

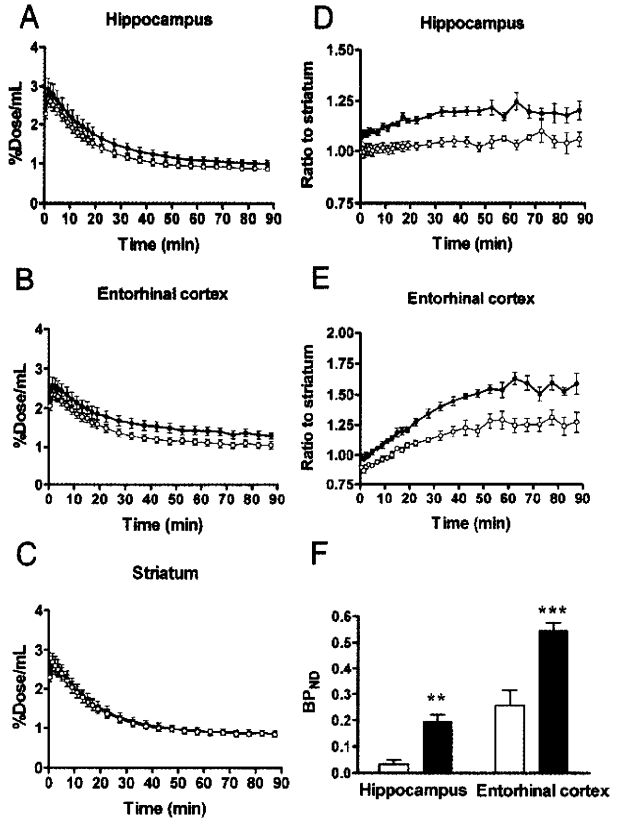

Figure 3. Kinetics of intravenously administered [^{11}C]AC-5216 in brains of 11-month-old nTg (open symbols; $n = 6$) and PS19 Tg (closed symbols; $n = 8$) mice. ***A–C***, Time-radioactivity curves in the hippocampus (***A***), entorhinal cortex (***B***), and striatum (***C***) obtained from dynamic PET scans. ***D***, ***E***, Target-to-cerebellum ratio of radioactivities in the hippocampus (***D***) and entorhinal cortex (***E***). ***F***, BP_{ND} values for radioligand binding to TSPO in the hippocampus and entorhinal cortex calculated by simplified reference tissue model. $^{**}p < 0.01$ and $^{***}p < 0.001$ by Bonferroni's multiple comparison after ANOVA. Error bars represent SE.

genotype) of APP23 mice compared with nTg mice. Although BP_{ND} values calculated by simplified reference tissue model were significantly increased in the neocortex and hippocampus of APP23 mice compared with nTg controls (Fig. 7*F*), the retention of [^{11}C]AC-5216 signals in the striatum of aged nTg exceeded those in the hippocampus and neocortex, potentially resulting in inaccurate BP_{ND} estimates. Thus, we reexamined the radiotracer binding by calculating DVRs. Similar to BP_{ND}, values of DVR for [^{11}C]AC-5216 in the hippocampus and neocortex of APP23 mice were significantly larger than those of nTg controls (data not shown; $F_{(1,24)} = 20.3$, $p < 0.001$ for main effect of genotype), but were much smaller than those of aged tau Tg mice. In addition, PET scans of these animals with [^{18}F]FEDAA1106 failed to detect differences in glial activities between the two genotype groups ($n = 7$; data not shown).

As in PS19 mice, hippocampal BP_{ND} for [^{11}C]AC-5216 was significantly correlated with age in 15 APP23 mice at 12–27 months of age (Fig. 8*A*) ($r^2 = 0.29$, $p < 0.05$ by Pearson's correlation coefficient), in agreement with progressive Aβ amyloidosis in these animals. Twelve of these Tg animals also received PET scans with [^{11}C]PIB, and amyloid deposition in the hippocampus and neocortex was detected as increased BP_{ND} values, which were significantly greater than those for [^{11}C]AC-5216 (Fig. 8*B*) ($F_{(1,44)} = 79.4$, $p < 0.001$ for main effect of radioligand). Furthermore, there was no significant correlation between hippocampal

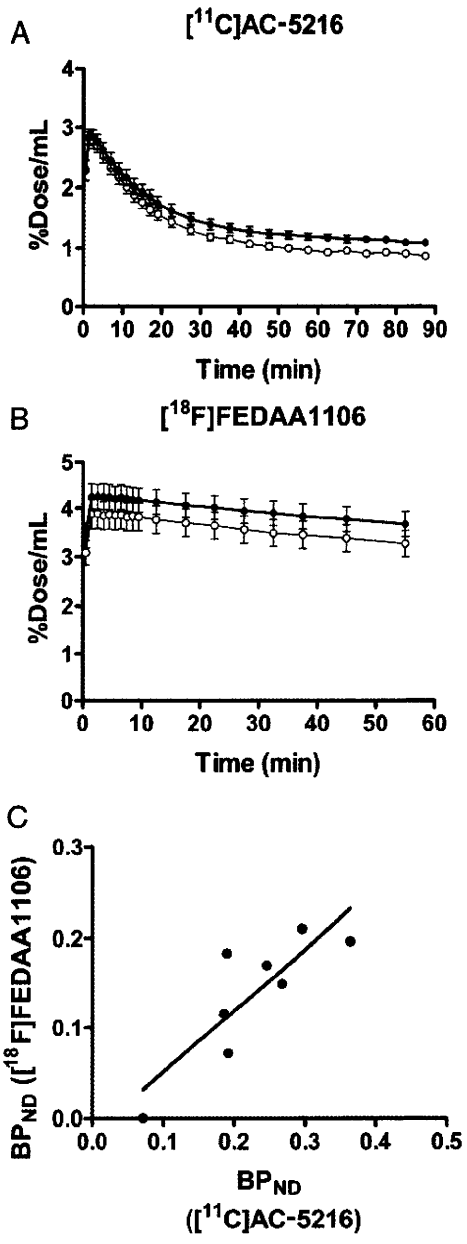

Figure 4. Comparison of brain kinetics and performance in detecting neuroinflammatory changes between two TSPO ligands, [^{11}C]AC-5216 and [^{18}F]FEDAA1106, in 11-month-old PS19 Tg mice ($n = 8$). ***A***, ***B***, Hippocampal (closed circles) and striatal (open circles) time-radioactivity curves in mice following intravenous injection of [^{11}C]AC-5216 (***A***) and [^{18}F]FEDAA1106 (***B***). Error bars represent SE. ***C***, Scatterplot of hippocampal BP_{ND} for [^{18}F]FEDAA1106 against that for [^{11}C]AC-5216 in each individual. Significant correlation between these BP_{ND} estimates was observed ($r^2 = 0.71$, $p < 0.01$ by *F* test), while [^{11}C]AC-5216 yielded larger values and better detectability of subtle inflammations than did [^{18}F]FEDAA1106. Solid line indicates the regression for all mice.

BP_{ND} values for these two radioligands (Fig. 8*C*) ($r^2 = 0.19$, $p > 0.05$ by Pearson's correlation coefficient), indicating that plaque deposition at a relatively early stage does not induce TSPO upregulation detectable in living brains.

TSPO upregulation following neuronal loss in $APP_{E693\Delta}$ mice

PET imaging of TSPO with [^{11}C]AC-5216 was also performed in 25.4-month-old $APP_{E693\Delta}$ mice, and radioligand retention was enhanced in the hippocampus and neocortex of these animals relative to age-matched controls (Fig. 9*A*). BP_{ND} values in the hippocampus

of $APP_{E693\Delta}$ mice ($n = 3$) was significantly greater than those of controls ($n = 5$) ($p < 0.05$ by t test). Postmortem assays demonstrated increased AT8 immunoreactivity in $APP_{E693\Delta}$ mice compared with nTg mice (data not shown), while the intensity of phosphor-tau immunolabeling in these Tg mice was much weaker than that in PS19 mice. TSPO signals were concentrated in putative glial cells in the hippocampus of $APP_{E693\Delta}$ mice (Fig. 9*B*), similar to PS19 mice (Yoshiyama et al., 2007; Ji et al., 2008). Based on quantification of hippocampal NeuN and TSPO immunoreactivities, $APP_{E693\Delta}$ mice presented neuronal loss, but did not exhibit detectable TSPO immunolabeling before the occurrence of notable neuronal death (Fig. 9*C*). This was in contrast with PS19 mice, in which TSPO-positive gliosis preceded pronounced neuronal loss (Fig. 9*C*).

Discussion

Notwithstanding the abundance of evidence for the activation of inflammatory glia in many neurodegenerative disorders, the roles of these cells in the propagation of and/or protection against neurotoxic injuries in the disease state are yet to be determined. In view of the present data obtained by the use of a high-contrast imaging agent, [^{11}C]AC-5216, and a newly generated antibody, microglial TSPO signals became detectable in living brains concomitant with accumulations of amyloid deposits as exemplified by fibrillar tau inclusions in neurons. Since TSPO immunoreactivities are associated with NFTs, neuropil threads, and plaque neurites rather than Aβ deposits, PET imaging of TSPO would provide a surrogate biomarker of tau-induced neuronal deteriorations in AD. This strategy also is applicable to non-AD tauopathies, in consideration of the numerous TSPO-positive microglia in PSP and Pick's disease brains and intense [^{11}C]AC-5216 radiosignals in PET scans of PS19 mice.

In vivo TSPO imaging may not be as capable of capturing early AD pathologies as amyloid PET with [^{11}C]PIB, because TSPO was not abundantly localized to AβN3pE-immunoreacitve diffuse plaques in AD brains, to which [^{11}C]PIB can firmly bind (Maeda et al., 2007; Higuchi et al., 2010). However, [^{11}C]AC-5216 could be more selective for proteinaceous aggregates that compromise neuronal survival like NFTs compared with plaques visualized by [^{11}C]PIB and other specific tracers. In fact, there have been multiple reports documenting 20–40% of nondemented elderly subjects with increased levels of [^{11}C]PIB

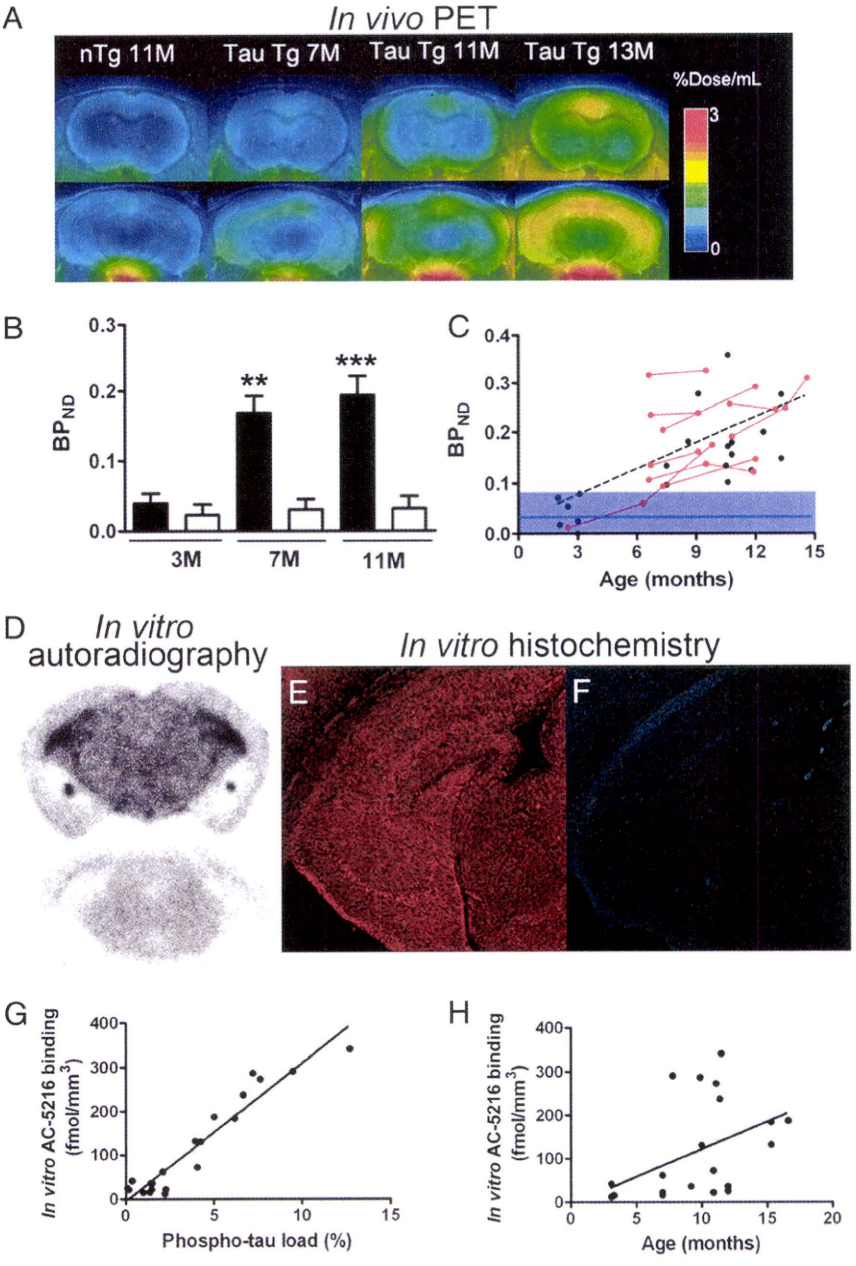

Figure 5. Progressive increase of PET and autoradiographic [^{11}C]AC-5216 signals in the hippocampus of PS19 mice as a function of age and phosphorylated tau load. ***A***, Coronal PET images containing the striatum (top) and hippocampus (bottom) in 11-month-old nTg and 7-, 11-, and 13-month-old PS19 Tg mice. Images were generated by averaging dynamic scan data at 30–90 min after radiotracer injection. ***B***, BP_{ND} for [^{11}C]AC-5216 in the hippocampus of nTg (open columns) and PS19 Tg (closed columns) mice at 3, 7, and 11 months of age. $^{**}p < 0.01$ and $^{***}p < 0.001$ by Bonferroni's multiple comparison after ANOVA. Error bars represent SE. ***C***, Scatterplot of hippocampal BP_{ND} for [^{11}C]AC-5216 against age in PS19 Tg mice ($n = 28$; mean age ± SD = 8.9 ± 3.4 months; age range, 2.2–14.6 months). Red symbols represent data from a longitudinal analysis of the same individuals ($n = 9$), and the blue line and purple area indicate the mean ± SD of hippocampal BP_{ND} values in nTg mice ($n = 17$; mean age ± SD = 7.5 ± 3.6 months; age range, 2–12 months). The increase of BP_{ND} in PS19 Tg mice became noticeable at ~6 months of age, and was thereafter augmented in a significant correlation with age ($r^2 = 0.40$, $p < 0.001$ by Pearson's correlation coefficient). The broken line denotes the regression in PS19 Tg mice. ***D***, Representative *in vitro* autoradiograms showing total (top section) and nonspecific (bottom section) binding of [^{11}C]AC-5216 in coronal brain slices obtained from a 12-month-old PS19 Tg mouse. Marked signal intensification was observed in the hippocampus, which exhibited severe atrophy. ***E***, ***F***, Double fluorescence labeling of the section shown in ***D*** with anti-phospho-tau antibody, AT8 (***E***), and amyloid dye, thioflavin-S (***F***). Numerous AT8-positive lesions lacking thioflavin-S positivity were present, and were conceived to be relatively immature intraneuronal amyloid fibrils. ***G***, ***H***, Scatterplots of autoradiographic [^{11}C]AC-5216 binding in the hippocampus of PS19 mice ($n = 21$) against AT8-positive phospho-tau load (***G***; expressed as percentage of total hippocampal area) and age (***H***). The solid lines represent regression.

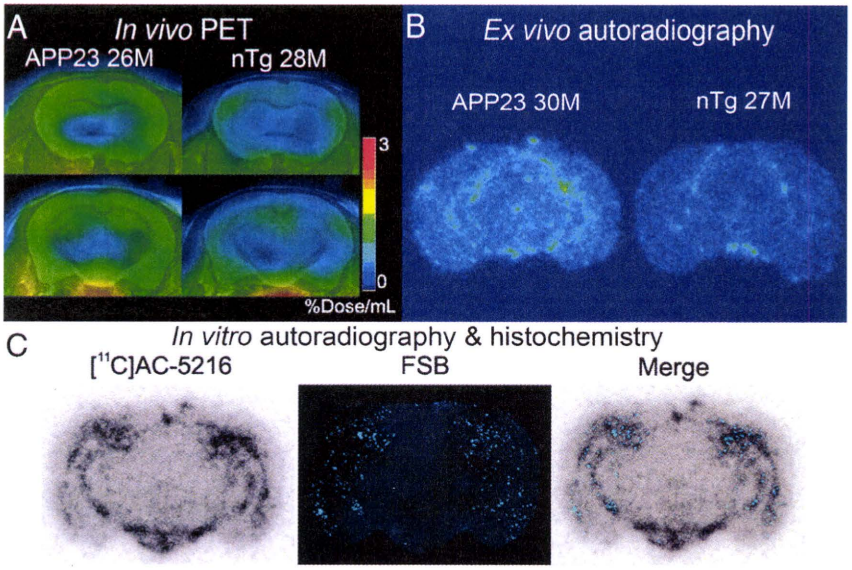

Figure 6. PET and autoradiographic images of TSPO upregulation in old APP23 mice. ***A***, Coronal PET images containing the striatum (top) and hippocampus (bottom) in 28-month-old nTg and 26-month-old APP23 Tg mice. Images were generated by averaging dynamic scan data at 30–60 min after [^{11}C]AC-5216 injection. ***B***, *Ex vivo* autoradiographic sections containing the hippocampus (at bregma −2.8 mm) in 27-month-old nTg and 30-month-old APP23 Tg mice. Brains were collected at 30 min after intravenous injection of [^{11}C]AC-5216. ***C***, Amyloidosis-associated *in vitro* autoradiographic [^{11}C]AC-5216 signals in a 24-month-old APP23 Tg mouse brain section. The autoradiographic section (left) was subsequently stained with an amyloid dye, FSB (middle), and colocalization of radiotracer binding and plaque deposition was assessed in a merged image (right).

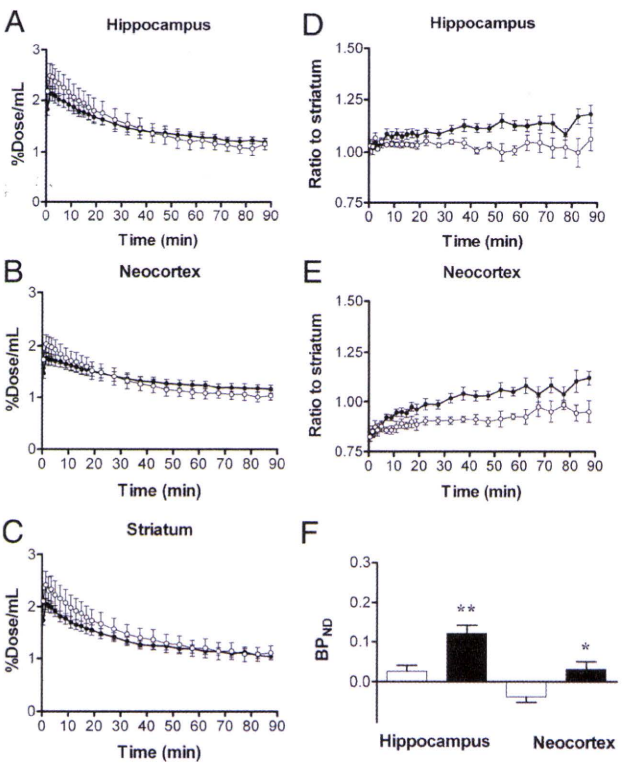

Figure 7. Kinetics of intravenously administered [^{11}C]AC-5216 in brains of 24-month-old nTg (open symbols; $n = 5$) and APP23 Tg (closed symbols; $n = 9$) mice. ***A–C***, Time-radioactivity curves in the hippocampus (***A***), entorhinal cortex (***B***), and striatum (***C***) obtained from dynamic PET scans. ***D***, ***E***, Target-to-cerebellum ratio of radioactivities in the hippocampus (***D***) and entorhinal cortex (***E***). ***F***, BP_{ND} values for radioligand binding to TSPO in the hippocampus and entorhinal cortex calculated by simplified reference tissue model. $^{*}p < 0.05$ and $^{**}p < 0.01$ by Bonferroni's multiple comparison after ANOVA. Error bars represent SE.

retention in the brain (Mintun et al., 2006; Pike et al., 2007; Jack et al., 2009), a factor that might hinder the use of amyloid imaging agents for selecting individuals requiring disease-modifying and/or neuroprotective treatments. Likewise, radiotracers for fibrillar tau aggregates in preclinical development stages (Okamura et al., 2005; Higuchi, 2009; Higuchi et al., 2010; Maruyama et al., 2009) are potentially advantageous over TSPO ligands in differentiating between tau-positive and tau-negative frontotemporal lobar degenerations, while [^{11}C]AC-5216 is likely to serve for visualizing neurotoxic events at a certain stage that PET with tau fibril agents may not cover. This notion is supported by our observation that thioflavin-S- and FSB-negative but AT8-positive phospho-tau inclusions were coexistent with autoradiographic [^{11}C]AC-5216 signals in PS19 mice. It is accordingly possible that relatively immature tau assemblies poorly captured by β-sheet ligands damage neurons and recruit TSPO-expressing microglia in response to this damage. The neurotoxicities induced by low-order tau multimers has been implicated in disease through studies of tau Tg mouse models (Higuchi et al., 2002; Santacruz et al., 2005; Yoshiyama et al., 2007), and the consequent TSPO-positive microgliosis is in sharp contrast with the lack of TSPO upregulation in microglia responding to extracellular Aβ deposits except neuritic plaques. Although dense-cored plaques in APP23 were found to be surrounded by astrocytes expressing TSPO (Ji et al., 2008), such astrocytic TSPO signals were undetectable in postmortem AD brains (Fig. 1*I*), indicating the absence of tight links between nonneuritic plaques and TSPO-positive gliosis in human cases. The astrocytic TSPO expression was positively correlated with glial cell-derived neurotrophic factor immunoreactivity across diverse animal models including APP23 mice (Ji et al., 2008). By contrast, our auxiliary analysis has shown that activated astrocytes in AD brains barely displayed this neurotrophic signal (data not shown) and thus could aggressively act on neurons in synergy with TSPO-positive microglia, unlike those in APP23 mice. This distinction between species concerning glial characteristics is attributable to neurodegenerative tau pathologies, which exist in AD but are uncommon in APP Tg mice. Furthermore, the presence of neurotoxic inflammation antecedent to the NFT deposition would also be examined in living humans with prodromal tauopathies by the concomitant use of radioligands for TSPO and tau fibrils.

It is of additional importance that an increase in TSPO levels was observed in the hippocampus of PS19 mice at 7 months of age despite the lack of MRI-measurable regional atrophies at this stage (Yoshiyama et al., 2007), and our recent PET study with [^{18}F]FEDAA1106 and [^{18}F]FDG has also demonstrated precedence of TSPO increases to impairments of cerebral glucose metabolism in PS19 mice (Hattori S, Maeda J, Tokunaga M, Yu I, Ji B, Ono M, Maruyama M, Aoki I, Zhang MR, Fukumura T, Suhara T, Higuchi M, unpublished observations). These findings collectively imply advantages of TSPO-PET over morphometric and metabolic imaging in detecting incipient neurotoxicities induced by tau abnormalities. This notion is further supported by the present neuropathological data demonstrating emergence of TSPO-expressing

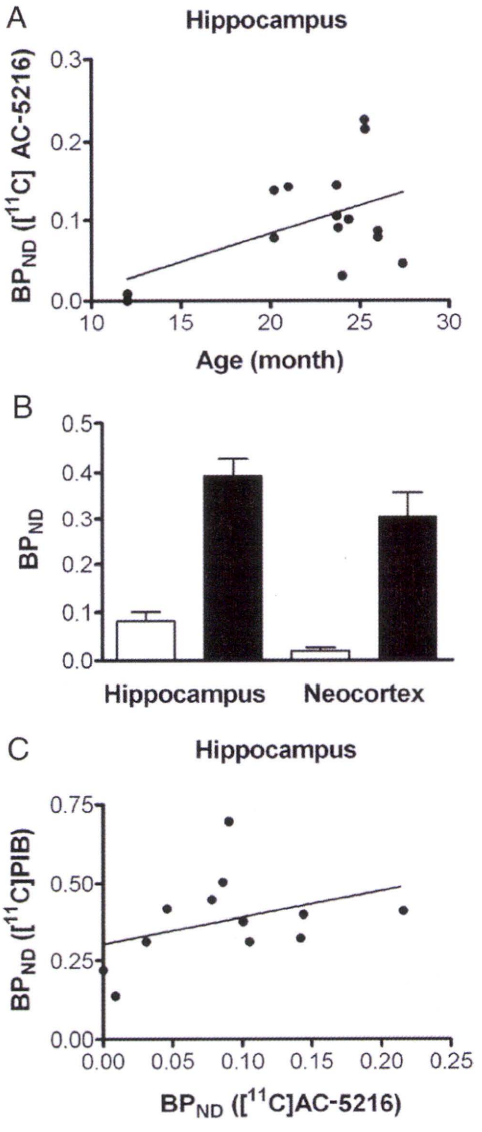

Figure 8. Association of TSPO signals with age-dependent deposition of Aβ amyloid in living brains of APP23 mice. ***A***, Scatterplot of BP_{ND} for [^{11}C]AC-5216 against age in the hippocampus of APP23 Tg mice ($n = 15$; mean age ± SD = 22.4 ± 4.9 months; age range, 12–28.4 months). The solid line represents regression. ***B***, BP_{ND} of [^{11}C]AC-5216 (open columns) and an amyloid radioligand, [^{11}C]PIB (closed columns), in the hippocampus of APP23 Tg mice ($n = 12$; mean age ± SD = 22.6 ± 5.3 months; age range, 12–28.4 months). Error bars represent SE. ***C***, Scatterplot of BP_{ND} for [^{11}C]PIB against that for [^{11}C]AC-5216 in the hippocampus of APP23 Tg mice ($n = 12$; mean age ± SD = 22.6 ± 5.3 months; age range, 12–28.4 months). The solid line represents regression.

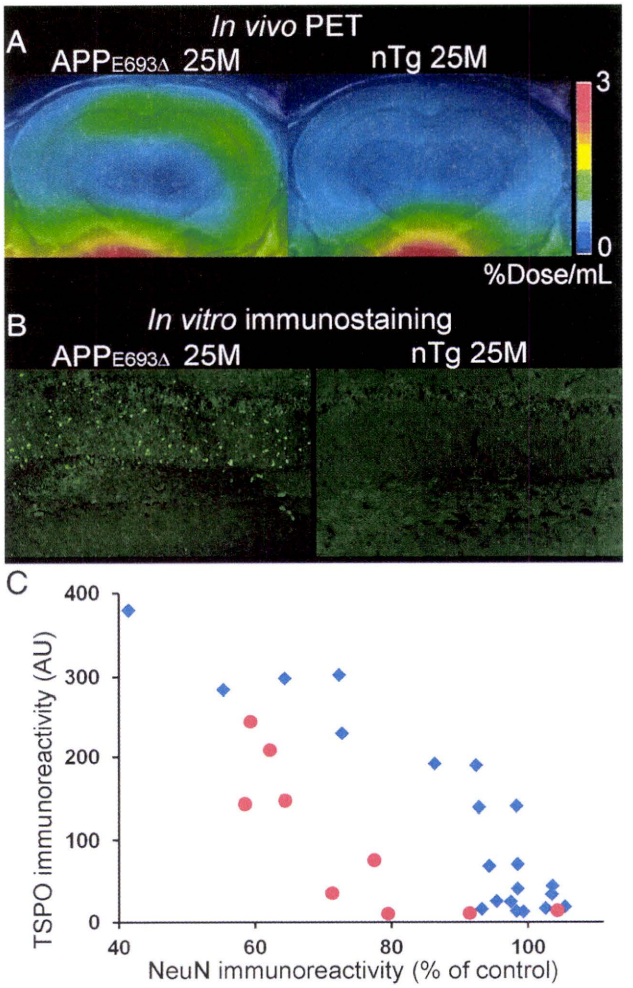

Figure 9. TSPO upregulation and neuronal loss in $APP_{E693\Delta}$ and PS19 mice. ***A***, Coronal PET images containing the hippocampus in 25.4-month-old $APP_{E693\Delta}$ Tg (left) and 25-month-old nTg (right) mice. Images were generated by averaging dynamic scan data at 30–60 min after [^{11}C]AC-5216 injection. ***B***, Immunolabeling of TSPO with NP155 in the hippocampal CA1 region of 25.4-month-old $APP_{E693\Delta}$ Tg (left; the same animal as shown in ***A***) and 25-month-old nTg (right) mice. ***C***, Intensity of TSPO immunolabeling (arbitrary values) plotted against NeuN immunoreactivity (percentage of area in controls matched by age with each individual) in $APP_{E693\Delta}$ (red circles; $n = 9$; 22–33 months of age) and PS19 mice (blue rhombuses; $n = 21$; 3–17 months of age).

glia antecedent to loss of NeuN signals in the hippocampus of PS19 mice, which is in distinction from increased TSPO levels apparently secondary to neuronal loss in $APP_{E693\Delta}$ mice, despite neurotoxicities of intraneuronal oligomeric Aβ-inducing gliotic changes at relatively young ages (Tomiyama et al., 2010). It is, however, yet to be clarified with different experimental models whether TSPO-positive glia is specifically responsive to tau lesions, or whether intracellular accumulation of some other pathologically involved molecules, such as α-synuclein (Spillantini et al., 1997) and TDP-43 (Neumann et al., 2006) can be a strong inducer of glial TSPO upregulation at an early stage of neurodegeneration.

Research attempts to incorporate PET imaging with [^{11}C]PK11195 in the clinical workup for AD have so far only proven its limited capability in discriminating afflicted patients from normal elderly (Cagnin et al., 2001; Edison et al., 2008; Okello et al., 2009; Wiley et al., 2009) and pathologically grading disease severity, but this shortcoming may reflect a relatively inefficient blood–brain barrier penetration and binding affinity of the radioligand (Maeda et al., 2004). A series of DAA1106 analogs, which yielded intense PET signals displaceable with nonradioactive TSPO ligands in the brains of rodents and primates (Maeda et al., 2004; Zhang et al., 2004; Venneti et al., 2007, 2008), have been reported to visualize increases of TSPO in AD brains (Yasuno et al., 2008), but these changes were not spatially linked to depositions of Aβ and tau fibrils. According to the small-animal PET data obtained here, [^{11}C]AC-5216 enables PET mapping of glial TSPO with a higher contrast than does [^{18}F]FEDAA1106 in AD model mice, benefiting from its prompt exit from the brain when unbound to the target-binding elements. Since Tg animals used here did not model the entire etiological pathway in the transition from aging to neurodegenerative disorders, the performance of [^{11}C]AC-5216 in humans relative to [^{18}F]FEDAA1106 is not fully predictable

according to the current data, and will need to be evaluated by clinical PET assessments.

Despite myriad evidences for interplays between dying neurons and inflammatory gliosis (Block et al., 2007), little is known concerning molecular signals mediating the stimulation of TSPO-positive microglia by phosphorylated tau depositions antecedent to overt neuronal loss, as observed in the previous *in vitro* autoradiographic (Yoshiyama et al., 2007) and present *in vivo* PET analyses. Upregulations of cyclooxygenase-2 (cox-2) and interleukin-1β (IL-1β) were indicated to be early pathological alterations in PS19 and similar tau Tg mouse strains (Bellucci et al., 2004; Yoshiyama et al., 2007), and a study on neuronal cell cultures reported that IL-1β could induce cox-2 expression (Hoozemans et al., 2001). In these considerations, it is inferable that proinflammatory cytokines exemplified by IL-1β are responsible for tau-triggered neuronal deteriorations. In addition to these neuroinflammatory pathologies, PS19 mice were characterized as initially developing abnormal tau accumulations in presynaptic terminals of hippocampal neurons (Yoshiyama et al., 2007). A speculative hypothesis that synaptic tau lesions are inducers of an inflammatory cascade could be drawn by linking these facts, since disruptions of synaptic functionality and calcium homeostasis may locally give rise to activation of NF-κB (Meffert et al., 2003), a multifunctional component capable of provoking transcriptions of proinflammatory cytokines. Conversion of microglia from resident and /or neuroprotective forms to an aggressive mode could consequently occur, and could be detected as overexpression of TSPO (Ji et al., 2008). Presynaptic degeneration and microgliosis were also observed as early pathological alterations in $APP_{E693\Delta}$ mice (Tomiyama et al., 2010), but were not concurrent with TSPO upregulation until the occurrence of neuronal death. As Aβ deposits in these animals were compartmentalized in endosomes, lysosomes, endoplasmic reticulum, and some other organelles (Nishitsuji et al., 2009), unlike cytoplasmic accumulation of tau proteins in PS19 mice (Yoshiyama et al., 2007), we presume that these Aβ species may initially provoke glial activation in a TSPO-negative mode distinct from tau-induced gliosis. TSPO can therefore be a biomarker for impending neuronal death accelerated by aggressive microglial response to tau lesions. This view may be in line with our recent observation of increased [^{18}F]FEDAA1106 signals in a subset of asymptomatic individuals carrying the tau gene mutation causative of familial tauopathy (Miyoshi et al., 2010), and the sensitivity of capturing early neuroinflammatory changes in such cases would be enhanced by applying [^{11}C]AC-5216 to clinical assays.

The tight interconnections between TSPO increase and tau-induced neurodegeneration as illustrated in the present work support the applicability of [^{11}C]AC-5216-PET to nonclinical and clinical evaluations of emerging anti-amyloid treatments. Aβ immunization, for instance, triggers activation of TSPO-positive glial cells (Maeda et al., 2007), which may contain microglia unengaged in plaque removal and be prone to promoting neurotoxic tau pathogenesis. *In vivo* monitoring of TSPO levels would play a pivotal role in determining the safety margin of therapeutic agents counteracting the Aβ accumulation. Similarly, active and passive immunization strategies under development now against phosphorylated tau proteins (Asuni et al., 2007; Takeuchi et al., 2009) possibly stimulate a toxic conversion of microglia accompanied by a surge of TSPO, and this issue would be addressed with the aid of TSPO-PET scans of treated animal models.

To conclude, we describe here the properties of a biomarker for microglia that is a sensitive reporter of neurotoxic effects of tau inclusion formation in AD and related neurodegenerative tauopathies based on a new class of TSPO radioligands. As the kinetics of [^{11}C]AC-5216 has been characterized in normal human subjects (Miyoshi et al., 2009), a side-by-side comparison would be enabled between courses of neuroinflammatory insults in humans and experimental models, toward the establishment of immunotherapeutic interventions in the disease pathogenesis and creation of better genetically engineered animals recapitulating the amyloidosis-gliosis intercontinuum in human diseases.

References

Asuni AA, Boutajangout A, Quartermain D, Sigurdsson EM (2007) Immunotherapy targeting pathological tau conformers in a tangle mouse model reduces brain pathology with associated functional improvements. J Neurosci 27:9115–9129.

Bellucci A, Westwood AJ, Ingram E, Casamenti F, Goedert M, Spillantini MG (2004) Induction of inflammatory mediators and microglial activation in mice transgenic for mutant human P301S tau protein. Am J Pathol 165:1643–1652.

Block ML, Zecca L, Hong JS (2007) Microglia-mediated neurotoxicity: uncovering the molecular mechanisms. Nat Rev Neurosci 8:57–69.

Cagnin A, Brooks DJ, Kennedy AM, Gunn RN, Myers R, Turkheimer FE, Jones T, Banati RB (2001) In-vivo measurement of activated microglia in dementia. Lancet 358:461–467.

Diorio D, Welner SA, Butterworth RF, Meaney MJ, Suranyi-Cadotte BE (1991) Peripheral benzodiazepine binding sites in Alzheimer's disease frontal and temporal cortex. Neurobiol Aging 12:255–258.

Dodel RC, Hampel H, Du Y (2003) Immunotherapy for Alzheimer's disease. Lancet Neurol 2:215–220.

Edison P, Archer HA, Gerhard A, Hinz R, Pavese N, Turkheimer FE, Hammers A, Tai YF, Fox N, Kennedy A, Rossor M, Brooks DJ (2008) Microglia, amyloid, and cognition in Alzheimer's disease: An [^{11}C](R)PK11195-PET and [^{11}C]PIB-PET study. Neurobiol Dis 32:412–419.

Higuchi M (2009) Visualization of brain amyloid and microglial activation in mouse models of Alzheimer's disease. Curr Alzheimer Res 6:137–143.

Higuchi M, Ishihara T, Zhang B, Hong M, Andreadis A, Trojanowski J, Lee VM (2002) Transgenic mouse model of tauopathies with glial pathology and nervous system degeneration. Neuron 35:433–446.

Higuchi M, Iwata N, Matsuba Y, Sato K, Sasamoto K, Saido TC (2005) ^{19}F- and ^{1}H-MRI detection of amyloid-β plaques in vivo. Nat Neurosci 8:527–533.

Higuchi M, Maeda J, Ji B, Maruyama M, Okauchi T, Tokunaga M, Ono M, Suhara T (2010) In-vivo visualization of key molecular processes involved in Alzheimer's disease pathogenesis: insights from neuroimaging research in humans and rodent models. Biochim Biophys Acta 1802:373–388.

Hoozemans JJ, Veerhuis R, Janssen I, Rozemuller AJ, Eikelenboom P (2001) Interleukin-1β induced cyclooxygenase 2 expression and prostaglandin E2 secretion by human neuroblastoma cells: implications for Alzheimer's disease. Exp Gerontol 36:559–570.

Jack CR Jr, Lowe VJ, Weigand SD, Wiste HJ, Senjem ML, Knopman DS, Shiung MM, Gunter JL, Boeve BF, Kemp BJ, Weiner M, Petersen RC (2009) Serial PIB and MRI in normal, mild cognitive impairment and Alzheimer's disease: implications for sequence of pathological events in Alzheimer's disease. Brain 132:1355–1365.

Ji B, Maeda J, Sawada M, Ono M, Okauchi T, Inaji M, Zhang MR, Suzuki K, Ando K, Staufenbiel M, Trojanowski JQ, Lee VM, Higuchi M, Suhara T (2008) Imaging of peripheral benzodiazepine receptor expression as biomarkers of detrimental versus beneficial glial responses in mouse models of Alzheimer's and other CNS pathologies. J Neurosci 28:12255–12267.

Klunk WE, Engler H, Nordberg A, Wang Y, Blomqvist G, Holt DP, Bergström M, Savitcheva I, Huang GF, Estrada S, Ausén B, Debnath ML, Barletta J, Price JC, Sandell J, Lopresti BJ, Wall A, Koivisto P, Antoni G, Mathis CA, Långström B (2004) Imaging brain amyloid in Alzheimer's disease with Pittsburgh Compound-B. Ann Neurol 55:306–319.

Lammertsma AA, Bench CJ, Hume SP, Osman S, Gunn K, Brooks DJ, Frackowiak RS (1996) Comparison of methods for analysis of clinical [^{11}C]raclopride studies. J Cereb Blood Flow Metab 16:42–52.

Logan J, Fowler JS, Volkow ND, Wang GJ, Ding YS, Alexoff DL (1996) Distribution volume ratios without blood sampling from graphical analysis of PET data. J Cereb Blood Flow Metab 16:834–840.

Maeda J, Suhara T, Zhang MR, Okauchi T, Yasuno F, Ikoma Y, Inaji M, Nagai Y, Takano A, Obayashi S, Suzuki K (2004) Novel peripheral benzodiaz-

epine receptor ligand [^{11}C]DAA1106 for PET: an imaging tool for glial cells in the brain. Synapse 52:283–291.

Maeda J, Ji B, Irie T, Tomiyama T, Maruyama M, Okauchi T, Staufenbiel M, Iwata N, Ono M, Saido TC, Suzuki K, Mori H, Higuchi M, Suhara T (2007) Longitudinal, quantitative assessment of amyloid, neuroinflammation, and anti-amyloid treatment in a living mouse model of Alzheimer's disease enabled by positron emission tomography. J Neurosci 27:10957–10968.

Maruyama M, Maeda J, Ji B, Zhang MR, Okauchi T, Ono M, Hattori S, Trojanowski JQ, Lee VMY, Fukumura T, Higuchi M, Suhara T (2009) *In-vivo* optical and PET detections of fibrillar tau lesions in a mouse model of tauopathies. In: 2009 Abstract Viewer/Itinerary Planner. Program No. IC-P-009. Alzheimer's Association International Conference on Alzheimer's Disease 2009, Chicago, July 2009.

McGeer PL, McGeer EG (1995) The inflammatory response system of brain: implications for therapy of Alzheimer and other neurodegenerative diseases. Brain Res Brain Res Rev 21:195–218.

Meffert MK, Chang JM, Wiltgen BJ, Fanselow MS, Baltimore D (2003) NF-κB functions in synaptic signaling and behavior. Nat Neurosci 6:1072–1078.

Mintun MA, Larossa GN, Sheline YI, Dence CS, Lee SY, Mach RH, Klunk WE, Mathis CA, DeKosky ST, Morris JC (2006) [^{11}C]PIB in a nondemented population: potential antecedent marker of Alzheimer disease. Neurology 67:446–452.

Miyoshi M, Ito H, Arakawa R, Takahashi H, Takano H, Higuchi M, Okumura M, Otsuka T, Kodaka F, Sekine M, Sasaki T, Fujie S, Seki C, Maeda J, Nakao R, Zhang MR, Fukumura T, Matsumoto M, Suhara T (2009) Quantitative analysis of peripheral benzodiazepine receptor in the human brain using PET with ^{11}C-AC-5216. J Nucl Med 50:1095–1101.

Miyoshi M, Shinotoh H, Wszolek ZK, Strongosky AJ, Shimada H, Arakawa R, Higuchi M, Ikoma Y, Yasuno F, Fukushi K, Irie T, Ito H, Suhara T (2010) In vivo detection of neuropathologic changes in presymptomatic *MAPT* mutation carriers: A PET and MRI study. Parkinsonism Relat Disord 16:404–408.

Neumann M, Sampathu DM, Kwong LK, Truax AC, Micsenyi MC, Chou TT, Bruce J, Schuck T, Grossman M, Clark CM, McCluskey LF, Miller BL, Masliah E, Mackenzie IR, Feldman H, Feiden W, Kretzschmar HA, Trojanowski JQ, Lee VM (2006) Ubiquitinated TDP-43 in frontotemporal lobar degeneration and amyotrophic lateral sclerosis. Science 314:130–133.

Nishitsuji K, Tomiyama T, Ishibashi K, Ito K, Teraoka R, Lambert MP, Klein WL, Mori H (2009) The E693Δ mutation in amyloid precursor protein increases intracellular accumulation of amyloid beta oligomers and causes endoplasmic reticulum stress-induced apoptosis in cultured cells. Am J Pathol 174:957–969.

Okamura N, Suemoto T, Furumoto S, Suzuki M, Shimadzu H, Akatsu H, Yamamoto T, Fujiwara H, Nemoto M, Maruyama M, Arai H, Yanai K, Sawada T, Kudo Y (2005) Quinoline and benzimidazole derivatives: candidate probes for in vivo imaging of tau pathology in Alzheimer's disease. J Neurosci 25:10857–10862.

Okello A, Edison P, Archer HA, Turkheimer FE, Kennedy J, Bullock R, Walker Z, Kennedy A, Fox N, Rossor M, Brooks DJ (2009) Microglial activation and amyloid deposition in mild cognitive impairment: a PET study. Neurology 72:56–62.

Pike KE, Savage G, Villemagne VL, Ng S, Moss SA, Maruff P, Mathis CA, Klunk WE, Masters CL, Rowe CC (2007) β-amyloid imaging and memory in non-demented individuals: evidence for preclinical Alzheimer's disease. Brain 130:2837–2844.

Santacruz K, Lewis J, Spires T, Paulson J, Kotilinek L, Ingelsson M, Guimaraes A, DeTure M, Ramsden M, McGowan E, Forster C, Yue M, Orne J, Janus C, Mariash A, Kuskowski M, Hyman B, Hutton M, Ashe KH (2005) Tau suppression in a neurodegenerative mouse model improves memory function. Science 309:476–481.

Sato K, Higuchi M, Iwata N, Saido TC, Sasamoto K (2004) Fluoro-substituted and ^{13}C-labeled styrylbenzene derivatives for detecting brain amyloid plaques. Eur J Med Chem 39:573–578.

Spillantini MG, Schmidt ML, Lee VM, Trojanowski JQ, Jakes R, Goedert M (1997) α-Synuclein in Lewy bodies. Nature 388:839–840.

Sturchler-Pierrat C, Abramowski D, Duke M, Wiederhold KH, Mistl C, Rothacher S, Ledermann B, Bürki K, Frey P, Paganetti PA, Waridel C, Calhoun ME, Jucker M, Probst A, Staufenbiel M, Sommer B (1997) Two amyloid precursor protein transgenic mouse models with Alzheimer disease-like pathology. Proc Natl Acad Sci U S A 94:13287–13292.

Tai YC, Ruangma A, Rowland D, Siegel S, Newport DF, Chow PL, Laforest R (2005) Performance evaluation of the microPET focus: a third-generation microPET scanner dedicated to animal imaging. J Nucl Med 46:455–463.

Takeuchi H, Inoue H, Higuchi M, Tsukita K, Trojanowski JQ, Lee VMY, Ji B, Takahashi R, Suhara T (2009) Development of therapies and monitoring for tauopathies with dementia. Soc Neurosci Abstr 35:236.16.

Tomiyama T, Matsuyama S, Iso H, Umeda T, Takuma H, Ohnishi K, Ishibashi K, Teraoka R, Sakama N, Yamashita T, Nishitsuji K, Ito K, Shimada H, Lambert MP, Klein WL, Mori H (2010) A mouse model of amyloid beta oligomers: their contribution to synaptic alteration, abnormal tau phosphorylation, glial activation, and neuronal loss *in vivo*. J Neurosci 30:4845–4856.

Trojanowski JQ (2008) PENN neurodegenerative disease research—in the spirit of Benjamin Franklin. NeuroSignals 16:5–10.

Venneti S, Lopresti BJ, Wang G, Slagel SL, Mason NS, Mathis CA, Fischer ML, Larsen NJ, Mortimer AD, Hastings TG, Smith AD, Zigmond MJ, Suhara T, Higuchi M, Wiley CA (2007) A comparison of the high-affinity peripheral benzodiazepine receptor ligands DAA1106 and (R)-PK11195 in rat models of neuroinflammation: implications for PET imaging of microglial activation. J Neurochem 102:2118–2131.

Venneti S, Wang G, Nguyen J, Wiley CA (2008) The positron emission tomography ligand DAA1106 binds with high affinity to activated microglia in human neurological disorders. J Neuropathol Exp Neurol 67:1001–1010.

Wiley CA, Lopresti BJ, Venneti S, Price J, Klunk WE, DeKosky ST, Mathis CA (2009) Carbon 11-labeled Pittsburgh Compound B and carbon 11-labeled (R)-PK11195 positron emission tomographic imaging in Alzheimer disease. Arch Neurol 66:60–67.

Yanamoto K, Kumata K, Yamasaki T, Odawara C, Kawamura K, Yui J, Hatori A, Suzuki K, Zhang MR (2009a) [^{18}F]FEAC and [^{18}F]FEDAC: Two novel positron emission tomography ligands for peripheral-type benzodiazepine receptor in the brain. Bioorg Med Chem Lett 19:1707–1710.

Yanamoto K, Yamasaki T, Kumata K, Yui J, Odawara C, Kawamura K, Hatori A, Inoue O, Yamaguchi M, Suzuki K, Zhang MR (2009b) Evaluation of N-benzyl-N-[^{11}C]methyl-2- (7-methyl-8-oxo-2-phenyl-7,8-dihydro-9H-purin-9-yl)acetamide ([^{11}C]DAC) as a novel translocator protein (18 kDa) radioligand in kainic acid-lesioned rat. Synapse 63:961–971.

Yasuno F, Ota M, Kosaka J, Ito H, Higuchi M, Doronbekov TK, Nozaki S, Fujimura Y, Koeda M, Asada T, Suhara T (2008) Increased binding of peripheral benzodiazepine receptor in Alzheimer's disease measured by positron emission tomography with [^{11}C]DAA1106. Biol Psychiatry 64:835–841.

Yoshiyama Y, Higuchi M, Zhang B, Huang SM, Iwata N, Saido TC, Maeda J, Suhara T, Trojanowski JQ, Lee VM (2007) Synapse loss and microglial activation precede tangles in a P301S tauopathy mouse model. Neuron 53:337–351.

Zhang MR, Maeda J, Ogawa M, Noguchi J, Ito T, Yoshida Y, Okauchi T, Obayashi S, Suhara T, Suzuki K (2004) Development of a new radioligand, N-(5-fluoro-2-phenoxyphenyl)-N-(2-[^{18}F]fluoroethyl-5-methoxybenzyl)acetamide, for pet imaging of peripheral benzodiazepine receptor in primate brain. J Med Chem 47:2228–2235.

Zhang MR, Kumata K, Maeda J, Yanamoto K, Hatori A, Okada M, Higuchi M, Obayashi S, Suhara T, Suzuki K (2007) ^{11}C-AC-5216: a novel PET ligand for peripheral benzodiazepine receptors in the primate brain. J Nucl Med 48:1853–1861.

Supplemental Materials

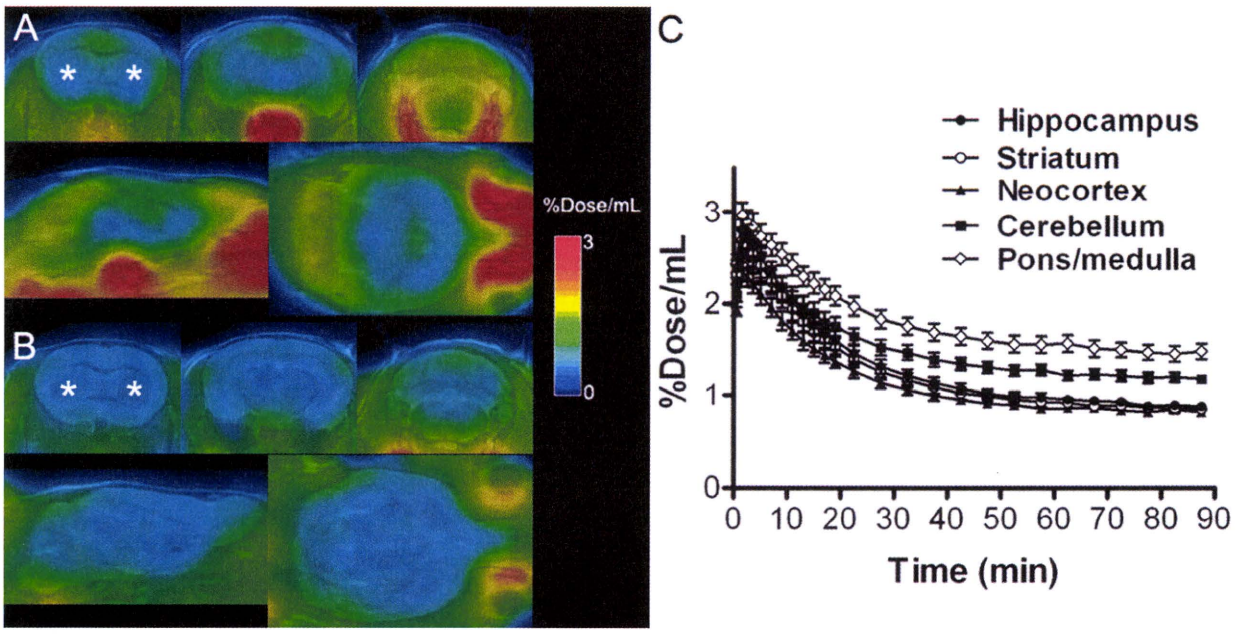

Supplemental Figure 1. Kinetics of [^{11}C]AC-5216 and its binding specificity in living nTg mouse brains. (A, B) Orthogonal views of [^{11}C]AC-5216 signals in brains of a nTg mouse scanned by PET at 30-90 min after intravenous injection of radioligand. Data were acquired at baseline (A) and following pretreatment with 5 mg/kg of PK11195 (B). Coronal images (upper panels) were generated to include the striatum (left; bregma +0.5 mm), hippocampus (middle; bregma -3.0 mm) and cerebellum (right; bregma -6.0 mm), and sagittal (lower left) and horizontal (lower right) slices were constructed at 1.0 mm lateral to the midline and 3.0 mm ventral to the bregma, respectively. PET maps are superimposed on the MRI anatomical template. Asterisks denote the striatum. (C) Time-radioactivity curves in multiple brain regions of nTg mice (n = 11; age range, 7 – 11 months).

Journal of Neuroscience Research

Journal of Neuroscience Research 89:1031–1042 (2011)

Intraneuronal Amyloid β Oligomers Cause Cell Death Via Endoplasmic Reticulum Stress, Endosomal/Lysosomal Leakage, and Mitochondrial Dysfunction In Vivo

Tomohiro Umeda,[1,2] Takami Tomiyama,[1,2]* Naomi Sakama,[1] Saya Tanaka,[1,3] Mary P. Lambert,[4] William L. Klein,[4] and Hiroshi Mori[1,2]*

[1]Department of Neuroscience, Osaka City University Graduate School of Medicine, Osaka, Japan
[2]Core Research for Evolutional Science and Technology, Japan Science and Technology Agency, Japan
[3]Yamaguchi University School of Medicine, Ube, Japan
[4]Department of Neurobiology and Physiology, Northwestern University, Evanston, Illinois

Intraneuronal accumulation of amyloid β (Aβ) is an early pathological change in Alzheimer's disease. Previously, we showed that the E693Δ mutation (referred to as the "Osaka" mutation) of amyloid precursor protein (APP) caused intracellular accumulation of Aβ oligomers and apoptosis in transfected COS-7 cells. We also showed that transgenic mice expressing $APP_{E693\Delta}$ (APP_{OSK}) displayed both an age-dependent accumulation of intraneuronal Aβ oligomers from 8 months of age and apparent neuronal loss in the hippocampus at 24 months of age. These findings indicate that intraneuronal Aβ oligomers cause cell death, but the mechanism of this process remains unclear. Accordingly, here we investigated the subcellular localization and toxicity of intraneuronal Aβ oligomers in APP_{OSK}-transgenic mice. We found Aβ oligomer accumulation in the endoplasmic reticulum (ER), endosomes/lysosomes, and mitochondria in hippocampal neurons of 22-month-old mice. We also detected up-regulation of Grp78 and HRD1 (an E3 ubiquitin ligase), leakage of cathepsin D from endosomes/lysosomes into cytoplasm, cytochrome c release from mitochondria, and activation of caspase-3 in the hippocampi of 18-month-old mice. Collectively, our findings suggest that intraneuronal Aβ oligomers cause cell death by inducing ER stress, endosomal/lysosomal leakage, and mitochondrial dysfunction in vivo.

Key words: Alzheimer's disease; APP E693Δ mutation; transgenic mouse

Extracellular soluble amyloid β (Aβ) oligomers are believed to cause synaptic and cognitive dysfunction in Alzheimer's disease (AD; Klein et al., 2001; Selkoe, 2002). However, mounting evidence has indicated that intraneuronal accumulation of Aβ is an early event in both AD (Gouras et al., 2000; Fernández-Vizarra et al., 2004) and Down syndrome (Gyure et al., 2001; Mori et al., 2002) and likely contributes to synaptic pathology (Hashimoto et al., 2003; Wirths et al., 2004; LaFerla et al., 2007; Gouras et al., 2010). In brains affected by AD, intraneuronal Aβ, which is predominantly in the form of Aβ42, has been shown to accumulate within certain organelles, including the endosomes/lysosomes (D'Andrea et al., 2001; Takahashi et al., 2002), autophagosomes (Yu et al., 2005), and mitochondria (Caspersen et al., 2005; Manczak et al., 2006). Intraorganelle accumulation of Aβ appears to damage these organelles and affects cell viability. For example, previous reports have shown that Aβ in endosomes/lysosomes underwent aggregation and disrupted membrane impermeability to induce endosomal/lysosomal leakage, which ultimately resulted in cell death (Yang et al., 1998; D'Andrea et al., 2001; Ditaranto et al., 2001; Ji et al., 2002; Takahashi et al., 2004; Hu et al., 2009; Friedrich et al., 2010). In addition, Aβ in autophagosomes has been shown to cause extensive accumulation of autophagic vesicles and subsequent autolysosomal leakage and neuronal death in *Drosophila* (Ling et al., 2009). Furthermore, Aβ in mitochondria was shown to disturb mitochondrial function and to cause apoptosis (Keil et al., 2004; Caspersen et al., 2005; Crouch et al., 2005; Manczak et al., 2006; Yao et al., 2009). In addition to these organelles, the endoplasmic reticulum (ER) is likely another target of

Contract grant sponsor: Ministry of Education, Culture, Sports, Science and Technology of Japan; Contract grant number: 21500352; Contract grant sponsor: Ministry of Health, Labour and Welfare, Japan; Contract grant sponsor: Alzheimer's Association; Contract grant number: IIRG-09-132098.

*Correspondence to: Takami Tomiyama, PhD or Hiroshi Mori, PhD, Department of Neuroscience, Osaka City University Graduate School of Medicine, 1-4-3 Asahimachi, Abeno-ku, Osaka 545-8585, Japan. E-mail: tomi@med.osaka-cu.ac.jp or mori@med.osaka-cu.ac.jp

Received 11 January 2011; Revised 4 February 2011; Accepted 8 February 2011

Published online 12 April 2011 in Wiley Online Library (wileyonlinelibrary.com). DOI: 10.1002/jnr.22640

intracellular Aβ, because increased ER stress and unfolded protein response (UPR) have been reported in brains affected by AD (Hoozemans et al., 2005).

We previously identified the E693Δ mutation (referred to as the "Osaka" mutation in the present study) in amyloid precursor protein (APP) from patients with familial AD (Tomiyama et al., 2008). This mutation, which corresponds to E22Δ in Aβ, was found to increase Aβ oligomerization but never showed Aβ fibrillization (Tomiyama et al., 2008). In transfected cells, this mutation failed to inhibit Aβ production but markedly reduced Aβ secretion by promoting intracellular accumulation of Aβ oligomers (Nishitsuji et al., 2009). The mutant Aβ localized to the ER, Golgi apparatus, endosomes, lysosomes, and autophagosomes and caused ER stress-induced apoptosis in transfected COS-7 cells (Nishitsuji et al., 2009). Enhanced accumulation of intracellular Aβ oligomers was also demonstrated in neurons of transgenic (Tg) mice expressing $APP_{E693\Delta}$ (also referred to as APP_{OSK}; Tomiyama et al., 2010). These mice displayed age-dependent synapse loss and abnormal tau phosphorylation, glial activation, and neuronal loss; however, they showed no extracellular amyloid deposition, even at 24 months of age. These findings suggest that intracellular Aβ, particularly its oligomeric form, plays a crucial role not only in synaptic pathology but also in neuronal death in AD. However, the mechanism underlying intraneuronal Aβ oligomer-induced cell death remains unclear. Although we previously demonstrated that intracellular Aβ oligomers cause ER stress-induced apoptosis in cultured cells, it is unknown whether this mechanism occurs in vivo. Furthermore, other mechanisms may also function in intracellular Aβ oligomer-induced neuronal death.

To address these questions, we investigated subcellular localization and toxicity of intraneuronal Aβ oligomers in APP_{OSK}-Tg mice. We focused on investigation of the ER, endosomes/lysosomes, and mitochondria and found that Aβ oligomers accumulated in all of these organelles. Furthermore, we detected increased signs of ER stress, endosomal/lysosomal leakage, mitochondrial dysfunction, and apoptosis. We discuss, based on these findings, the in vivo mechanisms of neuronal loss in terms of intraneuronal Aβ oligomers.

MATERIALS AND METHODS

Antibodies and Reagents

Mouse monoclonal antibody selective to Aβ oligomers (NU-1; Lambert et al., 2007) and rabbit polyclonal antibody to the C-terminal region of APP (C40; Suga et al., 2004) were prepared in our laboratories. Rabbit polyclonal antibody to Tom20, a mitochondria marker, was purchased from Santa Cruz Biotechnology (Santa Cruz, CA). Rabbit polyclonal antibodies to the E3 ubiquitin ligase HRD1 and actin were purchased from Sigma-Aldrich (St. Louis, MO). Rabbit polyclonal antibodies to calnexin, an ER marker, and Grp78, an ER-resident molecular chaperone, were purchased from Stressgen Bioreagents (Ann Arbor, MI). Rabbit polyclonal antibody to LAMP1, an endosome/lysosome marker, and mouse monoclonal antibodies to cathepsin D and cytochrome c were purchased from Abcam (Cambridge, United Kingdom). Mouse monoclonal antibody to cleaved caspase-3 was purchased from Cell Signaling Technology (Beverly, MA). A pinocytic tracer, Lucifer yellow, and a ratiometric dye, JC-1, were obtained from Molecular Probes-Invitrogen (Carlsbad, CA).

APP Constructs

Wild-type and Osaka-mutant human APP_{695} (APP_{WT} and APP_{OSK}, respectively) cDNA constructs were prepared with the pCI mammalian expression vector (Promega, Madison, WI) as described previously (Nishitsuji et al., 2009).

Animals

Eighteen- and twenty-two-month-old male and female APP_{OSK}-Tg line 1 mice (Tomiyama et al., 2010), APP_{WT}-Tg line 1 mice (Matsuyama et al., 2007), and the non-Tg littermates were used. The expression levels of human APP in the APP_{OSK}-Tg mice were about half the levels in the APP_{WT}-Tg mice (Tomiyama et al., 2010). All animal experiments were approved by the committee of Osaka City University and were performed in accordance with the Guide for Animal Experimentation, Osaka City University. Every effort was made to minimize the number of animals used and their suffering.

Immunocytochemistry

COS-7 cells grown on coverslips coated with poly-L-lysine were transfected with APP_{WT} or APP_{OSK} constructs using the Lipofectamine Plus reagent (Invitrogen). The cells were cultured overnight in 10% fetal calf serum/Opti-Mem I, and the media were replaced with serum-free Opti-Mem I. Three days after transfection, the cells were fixed with 4% paraformaldehyde in PBS at room temperature for 30 min and permeabilized by immersion in 0.05% Tween-20 in PBS for 3 sec. After being washed with PBS, the cells were blocked with 20% calf serum in PBS at room temperature for 1 hr. The cells were double stained with NU-1 and antibody to Tom20 at room temperature for 1 hr, followed by fluorescein isothiocyanate (FITC)-conjugated anti-mouse IgG antibody and rhodamine-conjugated anti-rabbit IgG antibody (Jackson Immunoresearch, West Grove, PA) at room temperature for 20 min. The stained specimens were mounted with the Vectashield mounting medium (Vector, Burlingame, CA) and viewed under a Leica TCS SP5 confocal laser microscope (Leica, Wetzlar, Germany).

For HRD1, cathepsin D, and cytochrome c staining, the cells at 3 days posttransfection were fixed and treated with 0.5% H_2O_2 at 4°C for 5 min to inactivate endogenous peroxidase. The cells were permeabilized, blocked, and stained with antibodies to HRD-1, cathepsin D, and cytochrome c followed by biotin-conjugated anti-rabbit or anti-mouse IgG antibody (Vector), horseradish peroxidase (HRP)-labeled avidin-biotin complex (ABC Elite; Vector), and the substrate DAB (Dojindo, Kumamoto, Japan). To examine the effect of extracellular Aβ on endosomal/lysosomal leakage, untransfected COS-7 cells grown on poly-L-lysine-coated coverslips

were cultured for 1 day in conditioned media obtained from APP-transfected COS-7 cells at 3 days posttransfection. These cultured cells were then fixed and stained with anticathepsin D antibody as described above. The stained specimens were viewed under a BX50 microscope (Olympus, Tokyo, Japan).

Immunohistochemistry

Brain sections were prepared from 18- and 22-month-old APP_{OSK}-Tg mice, APP_{WT}-Tg mice, and the non-Tg littermates as described previously (Tomiyama et al., 2010). We used 22-month-old sections for study on subcellular localization of Aβ oligomers but used 18-month-old sections for evaluation of toxicity of Aβ oligomers, because we wanted to know what organelle damage preceded the neuronal loss that occurred at 24 months of age (Tomiyama et al., 2010). The sections were pretreated by boiling in 0.01 N HCl (pH 2) for 10 min. After being washed with 100 mM Tris-HCl (pH 7.6) containing 150 mM NaCl (TBS), the sections were blocked with 20% calf serum in TBS for 1 hr. The sections were double stained with NU-1 and antibody to calnexin, LAMP1, or Tom20 at room temperature for 1 hr followed by FITC- and rhodamine-conjugated secondary antibodies at room temperature for 20 min. The sections were then treated with 0.1% Sudan black B in 70% ethanol at room temperature for 5 min to eliminate autofluorescence of lipofuscin. The stained specimens were viewed under a Leica TCS SP5 confocal laser microscope.

For cleaved caspase-3 staining, the sections were pretreated by boiling in 0.01 N HCl for 10 min, and, for staining of Grp78, HRD1, cathepsin D, and cytochrome c, the sections were pretreated by boiling in 10 mM citrate buffer (pH 5.5) for 30 min, followed by cooling for 10 min in a water bath and further incubation at room temperature for 30 min. After being washed with TBS, the sections were treated with 0.5% H_2O_2 at room temperature for 30 min. The sections were then blocked with 20% calf serum in TBS for 1 hr and stained with corresponding primary antibodies, followed by biotin-conjugated secondary antibodies, HRP-labeled ABC, and DAB. The stained specimens were viewed under a BX50 microscope.

Lucifer Yellow Staining

COS-7 cells at 3 days posttransfection cultured on poly-L-lysine-coated coverslips were incubated with 100 μg/ml Lucifer yellow in serum-free Opti-Mem I at 37°C for 2 hr. After being washed with PBS, the cells were mounted in PBS without fixation and viewed by fluorescence microscopy.

JC-1 Staining

COS-7 cells at 3 days posttransfection cultured on poly-L-lysine-coated coverslips were incubated with 1 μg/ml JC-1 in serum-free Opti-Mem I at 37°C for 20 min. After being washed with PBS, the cells were mounted in PBS without fixation and viewed by fluorescence microscopy.

Annexin V Staining

Apoptosis was examined using the Annexin V-FITC Apoptosis Detection Kit (BioVision, Mountain View, CA), which contains FITC-conjugated annexin V and a vital dye, propidium iodide. COS-7 cells at 3 days posttransfection cultured on poly-L-lysine-coated coverslips were incubated with an annexin V and propidium iodide mixture at room temperature for 5 min. After being washed with PBS, the cells were mounted in PBS without fixation and viewed by fluorescence microscopy.

Cytochrome c Release Assay

Cytochrome c release was evaluated using the Cytochrome c Releasing Apoptosis Assay Kit (BioVision, Inc.). COS-7 cells grown in 6-cm culture dishes were transfected with APP_{WT} and APP_{OSK} constructs and harvested 3 days after transfection. The resultant cells were homogenized in 400 μl of cytosol extraction buffer (supplied in the kit) using an ice-cold Dounce tissue grinder. After initial centrifugation at 700*g* for 10 min at 4°C, the supernatants were centrifuged again at 10,000*g* for 30 min at 4°C. The resultant supernatants were collected as cytosolic fractions, whereas the pellets were resuspended in 100 μl of the mitochondrial extraction buffer (supplied in the kit) and were saved as mitochondrial fractions. The protein content in each fraction was determined using the Pierce BCA Protein Assay Kit (Thermo Fisher Scientific, Rockford, IL). Samples with equal protein content were boiled in SDS sample buffer, subjected to SDS-PAGE with 12% NuPage Bis-Tris gels (Invitrogen), and transferred to Immobilon-P membranes (Millipore, Billerica, MA). After the membranes had been boiled in PBS for 10 min, cytochrome c was probed with its corresponding mouse monoclonal antibody (supplied in the kit), followed by HRP-labeled anti-mouse IgG antibody (Bio-Rad, Hercules, CA) and the chemiluminescent substrate Immobilon Western (Millipore). Signals were visualized using an LAS-3000 luminescent image analyzer (Fujifilm, Tokyo, Japan). Cell homogenates treated with SDS sample buffer were also subjected to Western blotting using 10% gels for detection of APP and actin.

The cytochrome c release assay was also performed using mouse hippocampal homogenates. Bilateral hippocampal tissues were dissected from 18-month-old APP_{OSK}-Tg mice and non-Tg littermates and were homogenized in 1 ml cytosol extraction buffer. After centrifugation at 700*g* for 10 min at 4°C, 800 μl of each supernatant was transferred into another tube and centrifuged again at 10,000*g* for 30 min at 4°C to separate the cytosol and mitochondria; the latter were further resuspended in 100 μl of the mitochondrial extraction buffer. Samples with equal protein content were subjected to Western blotting as described above. Signals of cytosolic cytochrome c were quantified using an LAS-3000 luminescent image analyzer.

Western Blotting of Grp78, Cathepsin D, and Caspase-3

Hippocampal homogenates and cytosolic fractions prepared from 18-month-old APP_{OSK}-Tg mice and non-Tg littermates were used to determine Grp78 induction, cathepsin D leakage, and caspase-3 activation. Samples with equal protein contents were subjected to Western blotting with antibodies to Grp78, cathepsin D, and the cleaved fragment of caspase-3. In some experiments, the membranes were also

stained with an antibody to actin to confirm that samples were loaded with equal protein content. Signals of Grp78 in homogenates, cathepsin D in cytosolic fractions, and activated caspase-3 in homogenates were quantified using an LAS-3000 luminescent image analyzer.

RESULTS

Aβ Oligomers Accumulated in the ER, Endosomes/Lysosomes, and Mitochondria

To investigate the mechanism underlying intraneuronal Aβ oligomer-induced cell death, we initially examined subcellular localization of Aβ oligomers in APP_{OSK}-Tg mouse brain. We focused on ER, endosomes/lysosomes, and mitochondria because these organelles have been shown to be the targets of Aβ. With transfected COS-7 cells, we had already obtained the result that Aβ oligomers accumulate in ER and endosomes/lysosomes (Nishitsuji et al., 2009). Thus, in the present study, we first examined whether Aβ oligomers also accumulate in mitochondria in these cells. Transfected COS-7 cells were stained with the Aβ oligomer-selective antibody NU-1 and antibody to the mitochondria marker Tom20. We found that Aβ oligomers accumulated in mitochondria and abundantly in APP_{OSK}-transfected cells, with none or little in mock- and APP_{WT}-transfected cells (Fig. 1A).

To study subcellular localization of Aβ oligomers in vivo, we prepared brain sections from 22-month-old APP_{OSK}-Tg mice, the age in which the mice displayed massive accumulation of intraneuronal Aβ oligomers in the hippocampus and cerebral cortex (Tomiyama et al., 2010), and from age-matched APP_{WT}-Tg mice and non-Tg littermates. The sections were stained with NU-1 and antibodies to the ER marker calnexin, endosome/lysosome marker LAMP1, and Tom20. Aβ oligomers were found to accumulate in ER, endosomes/lysosomes, and mitochondria in hippocampal neurons of the APP_{OSK}-Tg mice but not in the APP_{WT}-Tg mice and non-Tg littermates (Fig. 1B).

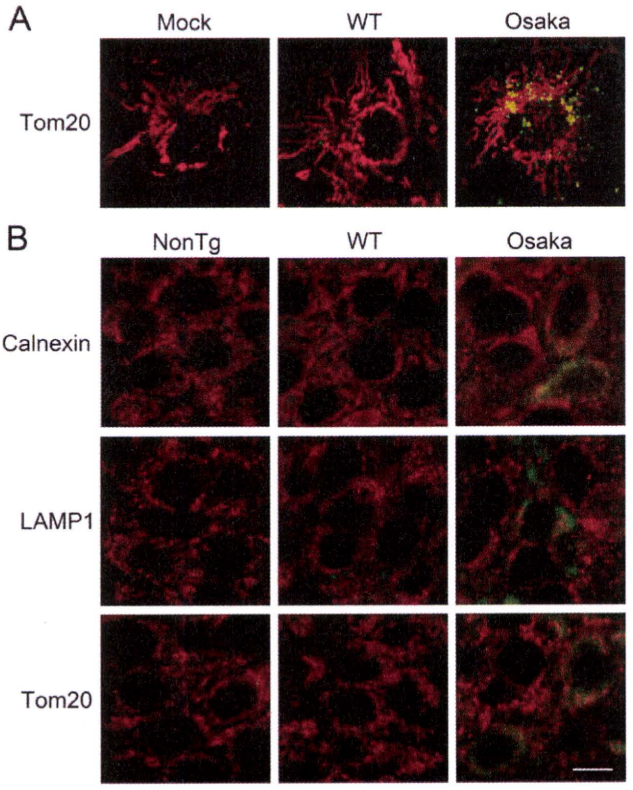

Fig. 1. Aβ oligomers accumulate in the ER, lysosomes, and mitochondria. **A:** COS-7 cells mock transfected or transfected with APP_{WT} (WT) or APP_{OSK} (Osaka) were double stained with Aβ oligomer-selective antibody NU-1 (green) and antibody to Tom20 (mitochondria; red). APP_{OSK}-transfected cells displayed abundant accumulation of Aβ oligomers in the mitochondria. **B:** Brain sections of 22-month-old APP_{OSK}-Tg mice (Osaka), APP_{WT}-Tg mice (WT), and non-Tg littermates (NonTg) were double stained with NU-1 (green) and antibodies to calnexin (ER), LAMP1 (endosomes/lysosomes), and Tom20 (red). Aβ oligomer accumulation was observed in the ER, endosomes/lysosomes, and mitochondria in hippocampal neurons of APP_{OSK}-Tg mice. The photographs show the hippocampal CA3 regions. Scale bar = 10 μm.

Aβ Oligomers Induced ER-Associated Degradation

Accumulation of Aβ oligomers in ER is expected to cause ER stress, and indeed we previously demonstrated that ER stress was prominently induced in APP_{OSK}-transfected cells (Nishitsuji et al., 2009). This was supported by enhanced induction of the molecular chaperone Grp78 and increased phosphorylation (i.e., inactivation) of the translation initiation factor eIF2α. In addition to these responses, ER stress typically elicits another response, called *ER-associated degradation* (ERAD; Yoshida, 2007). ERAD mediates ubiquitination of misfolded proteins and their translocation to proteasomes in the cytoplasm of cells. An E3 ubiquitin ligase, HRD1, also known as *SYVN1* (for synovial apoptosis inhibitor 1) or synoviolin, is a primary component of this process, and it has been reported that its level is increased during ER stress (Kikkert et al., 2004). Thus, we first examined HRD1 expression in transfected COS-7 cells by immunocytochemistry. Compared with mock- and APP_{WT}-transfected cells, APP_{OSK}-transfected cells displayed intense and diffuse immunoreactivity to HRD1 (Fig. 2A), indicating an enhanced induction of ERAD.

To test in vivo occurrence of Aβ oligomer-induced ER stress, we examined expression of Grp78 and HRD1 in the brains of 18-month-old APP_{OSK}-Tg mice by immunohistochemistry. Compared with the age-matched non-Tg littermates and APP_{WT}-Tg mice, the APP_{OSK}-Tg mice exhibited intense immunoreactivities to Grp78 (Fig. 2B) and HRD1 (Fig. 2C) in their hippocampal neurons. Increased intensity of neuronal Grp78 and HRD1 was also observed in the cerebral cortex of the APP_{OSK}-Tg mice (data not shown). We also examined the levels of Grp78 in hippocampal homogenates of 18-month-old APP_{OSK}-Tg mice and non-Tg

littermates. We detected increased levels of Grp78 in the Tg mice by Western blotting (Fig. 2D,E). Thus, these results demonstrated that ER stress was induced in vivo in association with ER accumulation of Aβ oligomers.

Aβ Oligomers Caused Endosomal/Lysosomal Leakage

It has been shown that exogenously applied Aβ causes endosomal/lysosomal leakage in neuronal cells (Yang et al., 1998; Ditaranto et al., 2001; Ji et al., 2002). We examined whether endosomal/lysosomal leakage is induced by endogenously generated Aβ oligomers. Initially, transfected COS-7 cells were incubated with the pinocytic tracer Lucifer yellow and were inspected in terms of subcellular distribution. In mock- and APP_{WT}-transfected cells, Lucifer yellow localized into intracellular puncta, which indicates that the tracer remained within the endocytic vesicles after internalization (Fig. 3A). In contrast, APP_{OSK}-transfected cells exhibited a diffuse distribution of Lucifer yellow throughout the cell body, with a few faint, punctate localizations, which indicates that endosomal/lysosomal membrane impermeability was disrupted. To confirm this finding, we further examined the subcellular distribution of the late endosome/lysosome-specific enzyme cathepsin D. Again, we found only punctate staining of cathepsin D in both mock- and APP_{WT}-transfected cells, whereas a diffuse distribution of cathepsin D was present throughout the cell body in APP_{OSK}-transfected cells (Fig. 3B).

We also examined whether this observed membrane disruption was caused by endocytosis of extracellular Aβ. We cultured untransfected COS-7 cells for 1 day in conditioned media obtained from APP-transfected cells and subsequently stained them with anticathepsin D antibody. Punctate staining of cathepsin D was observed in cells treated with mock- and APP_{WT}-conditioned media, whereas diffuse distribution was seen in cells treated with APP_{OSK}-conditioned media (Fig. 3C). These results indicate that endosomal/lysosomal leakage was induced, at least in part, by Aβ taken up from the extracellular space.

To examine the in vivo occurrence of Aβ oligomer-induced endosomal/lysosomal leakage, we initially examined the subcellular distribution of cathepsin D in the brains of 18-month-old APP_{OSK}-Tg mice by immunohistochemistry. We found only punctate staining of cathepsin D within the hippocampal neurons in age-matched non-Tg littermates and APP_{WT}-Tg mice, whereas we saw a diffuse distribution of cathepsin D throughout the cell bodies in APP_{OSK}-Tg mice (Fig. 3D). Some neurons exhibited intense immunoreactivity to cathepsin D in the hippocampus of APP_{OSK}-Tg mice. Similar images were also obtained in the cerebral cortex

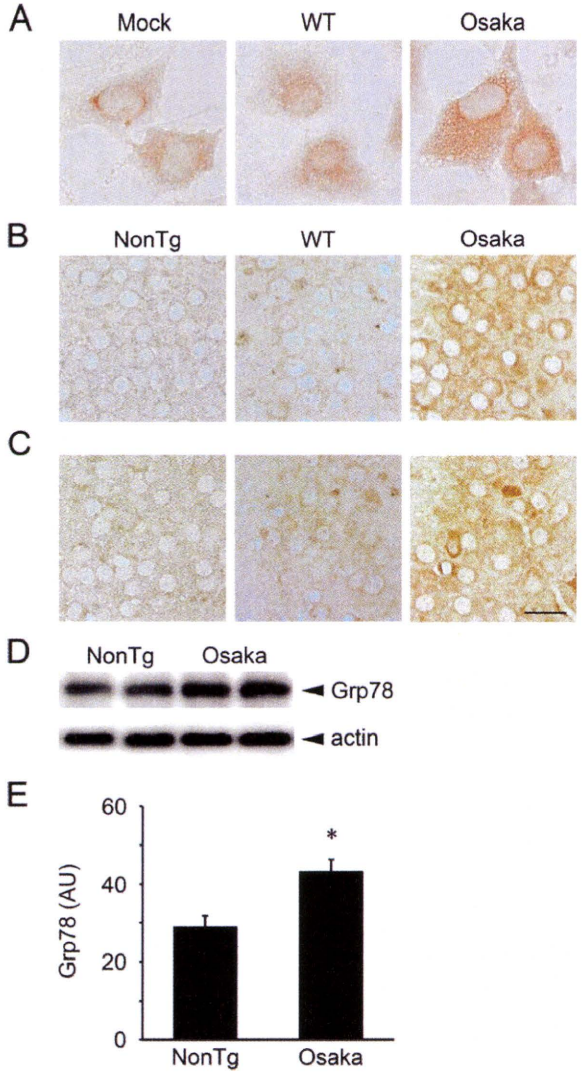

Fig. 2. Intracellular Aβ oligomers cause ER stress. **A:** COS-7 cells mock transfected or transfected with APP_{WT} (WT) or APP_{OSK} (Osaka) were stained with an antibody to the E3 ubiquitin ligase HRD1. Compared with mock- and APP_{WT}-transfected cells, the APP_{OSK}-transfected cells displayed intense and diffuse immunoreactivity to HRD1, indicating an enhanced induction of the ER-associated degradation (ERAD) in APP_{OSK}-transfected cells. **B,C:** Brain sections of 18-month-old APP_{OSK}-Tg mice (Osaka), APP_{WT}-Tg mice (WT), and non-Tg littermates (NonTg) were stained with antibodies to the ER resident molecular chaperone Grp78 (B) and HRD1 (C). Compared with non-Tg littermates and APP_{WT}-Tg mice, the APP_{OSK}-Tg mice exhibited intense immunoreactivities to Grp78 and HRD1. The photographs show the hippocampal CA3 regions. **D,E:** Hippocampal homogenates with equal protein content of 18-month-old APP_{OSK}-Tg mice and non-Tg littermates were subjected to Western blotting for Grp78. An increased level of Grp78 was detected in APP_{OSK}-Tg mice. No difference in actin level was observed among samples, confirming that samples were loaded with equal protein content. The figure shows representative blots. E: The signals of Grp78 were quantified and expressed in arbitrary units (AU) per lane. Each result is presented as the mean ± SE (n = 5). $^{\star}P = 0.0099$ vs. non-Tg by unpaired Student's *t*-test. Scale bar = 20 μm.

of the APP_{OSK}-Tg mice (data not shown). We also examined the levels of cathepsin D that leaked from endosomes/lysosomes into cytoplasm in the hippocampi of 18-month-old APP_{OSK}-Tg mice and non-Tg littermates. Hippocampal cytosolic fractions were prepared, and the levels of cathepsin D were evaluated by Western blotting. Compared with non-Tg littermates, the Tg mice exhibited increased levels of cytosolic cathepsin D (Fig. 3E,F). Thus, these results show that endosomal/lysosomal leakage occurs in vivo in association with endosomal/lysosomal accumulation of Aβ oligomers.

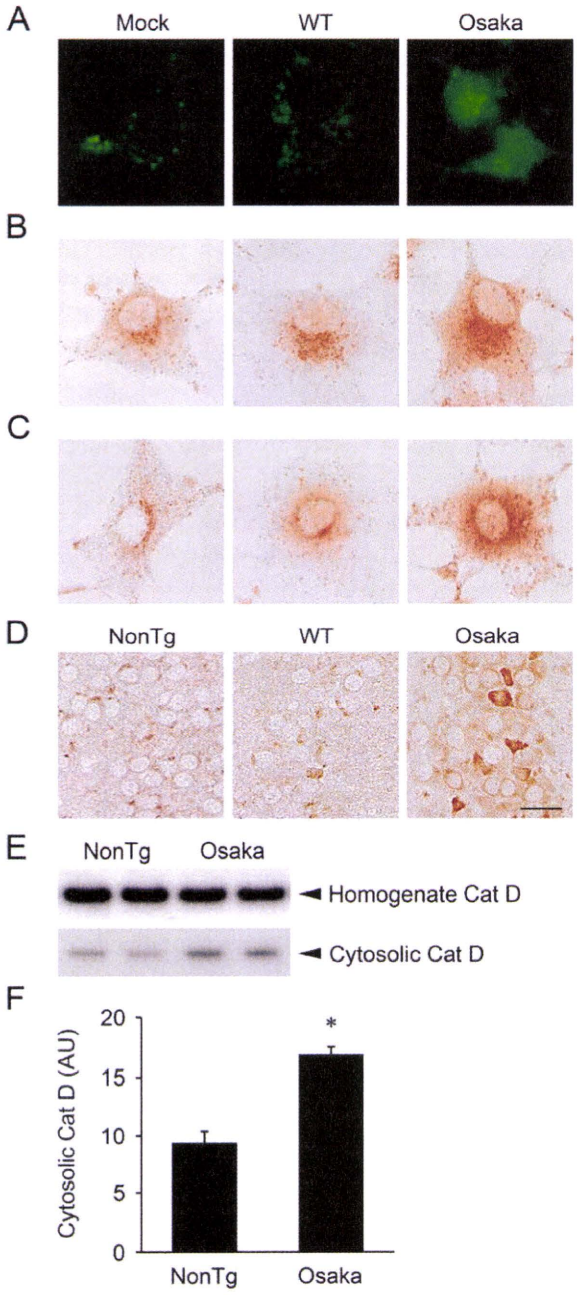

Fig. 3. Intracellular Aβ oligomers cause endosomal/lysosomal leakage. **A:** COS-7 cells mock transfected or transfected with APP_{WT} (WT) or APP_{OSK} (Osaka) were incubated with the pinocytic tracer Lucifer yellow. Mock- and APP_{WT}-transfected cells showed punctate localization of Lucifer yellow, whereas APP_{OSK}-transfected cells displayed a diffuse distribution of this probe throughout the cell body, indicating a disruption of endosomal/lysosomal membrane impermeability in APP_{OSK}-transfected cells. **B:** Transfected COS-7 cells were stained with an antibody to lysosomal enzyme cathepsin D. Again, mock- and APP_{WT}-transfected cells showed punctate localization of cathepsin D, whereas APP_{OSK}-transfected cells displayed a diffuse distribution of cathepsin D throughout the cell body, confirming the occurrence of endosomal/lysosomal leakage in APP_{OSK}-transfected cells. **C:** Untransfected COS-7 cells were cultured for 1 day in conditioned media obtained from mock-, APP_{WT}-, and APP_{OSK}-transfected cells and then stained with anticathepsin D antibody. Punctate distribution of cathepsin D was seen in cells treated with mock- and APP_{WT}-conditioned media, whereas diffuse distribution was observed in cells treated with APP_{OSK}-conditioned media, revealing that Aβ taken up from the extracellular space contributed to endosomal/lysosomal leakage. **D:** Brain sections of 18-month-old APP_{OSK}-Tg mice (Osaka), APP_{WT}-Tg mice (WT), and non-Tg littermates (NonTg) were stained with anticathepsin D antibody. Only punctate staining of cathepsin D was seen within the hippocampal neurons in APP_{WT}-Tg mice and non-Tg littermates, whereas a diffuse distribution of cathepsin D throughout the cell body was observed in APP_{OSK}-Tg mice. The photographs show the hippocampal CA3 regions. **E,F:** Hippocampal homogenates and cytosolic fractions with equal protein content of 18-month-old APP_{OSK}-Tg mice and non-Tg littermates were subjected to Western blotting for cathepsin D (Cat D). Increased levels of cytosolic cathepsin D were detected in APP_{OSK}-Tg mice. The figure shows representative blots. F: The signals of cytosolic cathepsin D were quantified and expressed in arbitrary units (AU) per lane. Each result is presented as the mean ± SE (n = 5). $\star P = 0.0004$ vs. non-Tg by unpaired Student's *t*-test. Scale bar = 20 μm.

Aβ Oligomers Caused Mitochondrial Dysfunction

It has been reported that Aβ accumulated in mitochondria in both AD and transgenic mouse brains, and in APP-transfected cells in association with mitochondrial dysfunction (Keil et al., 2004; Caspersen et al., 2005; Crouch et al., 2005; Manczak et al., 2006; Yao et al., 2009). Mitochondrial dysfunction includes changes in the membrane potential and leads to the release of cytochrome c from mitochondrial intermembrane space into the cytoplasm, the latter of which is a sign of mitochondria-dependent apoptosis. Accordingly, we first examined mitochondrial membrane potential in transfected COS-7 cells stained with JC-1. With mock- and APP_{WT}-transfected cells, we observed red fluorescence of characteristic punctate points/rods resulting from J-aggregate formation along with green fluorescence, indicating that mitochondrial membranes were intact (Fig. 4A). In contrast, APP_{OSK}-transfected cells showed the loss of red fluorescence and cytoplasmic diffusion of green fluorescence, indicating that mitochondrial membranes were aberrantly depolarized. Subsequently, we

examined whether cytochrome c was released in transfected COS-7 cells. Initially, subcellular distribution of cytochrome c was examined by immunocytochemistry. In both mock- and APP_{WT}-transfected cells, cytochrome c localized in mitochondrial networks that appeared healthy and intact (Fig. 4B). In contrast, APP_{OSK}-transfected cells displayed the loss of the network distribution of cytochrome c and instead showed a diffuse distribution of cytochrome c throughout the cell body, with a great deal of fragmented, blebby staining, which indicates both that mitochondrial structure was disrupted and that cytochrome c was released into the cytoplasm.

Accordingly, we also examined the levels of cytochrome c released from mitochondria into cytoplasm. Cell homogenates were separated into mitochondrial and cytosolic fractions, and the levels of cytochrome c were evaluated by Western blotting. Compared with the mock- and APP_{WT}-transfected cells, the APP_{OSK}-transfected cells exhibited increased levels of cytosolic cytochrome c (Fig. 4C). Taken together, these results indicate that severe mitochondrial damage occurs in APP_{OSK}-transfected cells.

To investigate the in vivo occurrence of Aβ oligomer-induced mitochondrial dysfunction, we examined the subcellular distribution of cytochrome c in the brains of 18-month-old APP_{OSK}-Tg mice by immuno-

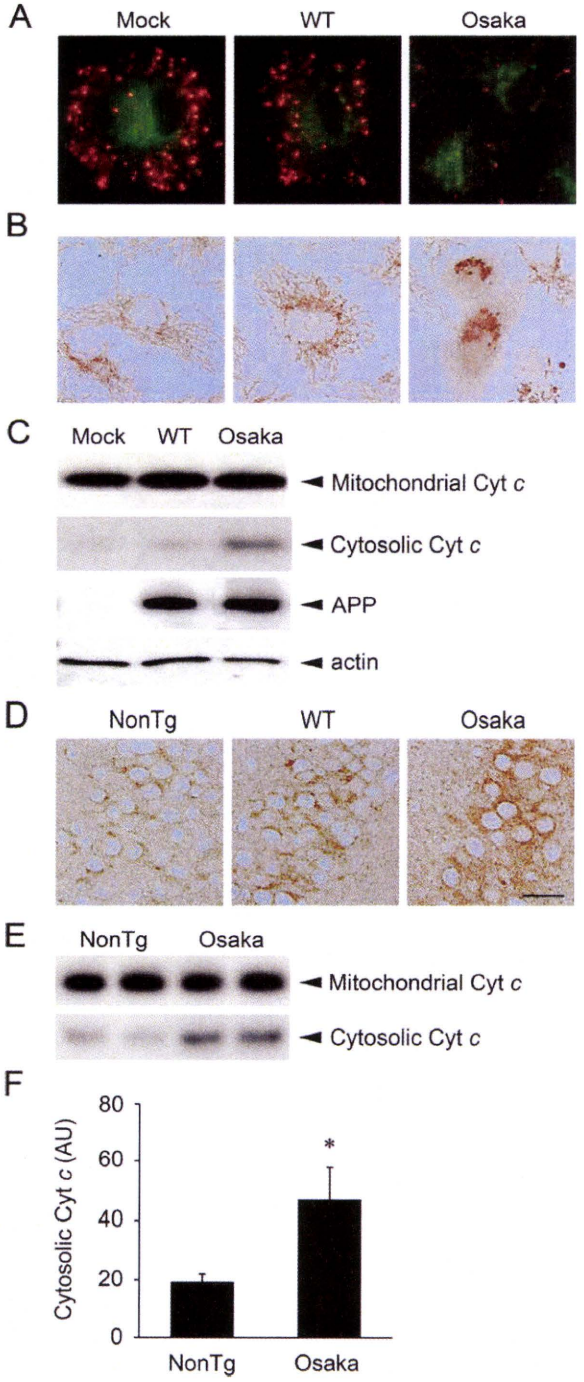

Fig. 4. Intracellular Aβ oligomers cause mitochondrial dysfunction. **A:** COS-7 cells mock transfected or transfected with APP_{WT} (WT) or APP_{OSK} (Osaka) were stained with JC-1, a reporter dye for mitochondrial condition. Mock- and APP_{WT}-transfected cells showed red fluorescence resulting from J-aggregate formation along with green fluorescence. In contrast, APP_{OSK}-transfected cells displayed a loss of red fluorescence and cytoplasmic diffusion of green fluorescence, indicating that mitochondrial membranes were aberrantly depolarized in APP_{OSK}-transfected cells. **B:** Transfected COS-7 cells were stained with an antibody to cytochrome c. Mock- and APP_{WT}-transfected cells showed a localization of cytochrome c in the mitochondrial network, whereas APP_{OSK}-transfected cells displayed a loss of network localization of cytochrome c and a diffuse distribution of cytochrome c throughout the cell body, with high levels of fragmented, blebby staining. These results indicate that mitochondrial structure was disrupted and cytochrome c was released into the cytoplasm in APP_{OSK}-transfected cells. **C:** Mitochondrial and cytosolic fractions with equal protein content prepared from transfected COS-7 cells were subjected to Western blotting for cytochrome c (Cyt c). Increased levels of cytosolic cytochrome c were detected in APP_{OSK}-transfected cells. Cell homogenates with equal protein content were also subjected to Western blotting for APP and actin. No difference in APP expression level was observed between APP_{WT}- and APP_{OSK}-transfected cells. The figure shows representative blots. **D:** Brain sections of 18-month-old APP_{OSK}-Tg mice (Osaka), APP_{WT}-Tg mice (WT), and non-Tg littermates (NonTg) were stained with anticytochrome c antibody. Only punctate staining of cytochrome c was seen within the hippocampal neurons in APP_{WT}-Tg mice and non-Tg littermates, whereas a diffuse distribution of cytochrome c throughout the cell body was observed in APP_{OSK}-Tg mice. The photographs show the hippocampal CA3 regions. **E,F:** Mitochondrial and cytosolic fractions with equal protein content prepared from the hippocampi of 18-month-old APP_{OSK}-Tg mice and non-Tg littermates were subjected to Western blotting for cytochrome c. Increased levels of cytosolic cytochrome c were detected in APP_{OSK}-Tg mice. The figure shows representative blots. F: The signals of cytosolic cytochrome c were quantified and expressed in arbitrary units (AU) per lane. Each result is presented as the mean ± SE (n = 5). $\star P = 0.0394$ vs. non-Tg by unpaired Student's *t*-test. Scale bar = 20 μm.

histochemistry. We observed only punctate staining of cytochrome c within the hippocampal neurons in age-matched non-Tg littermates and APP_{WT}-Tg mice, whereas we found a diffuse distribution of cytochrome c throughout the cell bodies in APP_{OSK}-Tg mice (Fig. 4D). Similar images were obtained in the cerebral cortex of the APP_{OSK}-Tg mice (data not shown). We also examined the levels of cytochrome c released from mitochondria into cytoplasm in the hippocampi of 18-month-old APP_{OSK}-Tg mice and non-Tg littermates. Hippocampal homogenates were separated into mitochondrial and cytosolic fractions, and the levels of cytochrome c were evaluated by Western blotting. Again, we detected increased levels of cytosolic cytochrome c in the Tg mice (Fig. 4E,F). Thus, these results show that mitochondrial dysfunction was induced in vivo in association with mitochondrial accumulation of Aβ oligomers.

Aβ Oligomers Caused Apoptosis

We previously demonstrated that the APP Osaka mutation caused intracellular accumulation of Aβ oligomers that resulted in ER stress-induced apoptosis in COS-7 cells (Nishitsuji et al., 2009). This was supported by activation of caspase-3 and −4 and DNA fragmentation. In the present study, we found that this mutation also induced endosomal/lysosomal leakage and mitochondrial dysfunction, both of which have been shown to result in cell death. Thus, we studied apoptosis in brains of APP_{OSK}-Tg mice. Initially, we confirmed our previous findings. Transfected COS-7 cells were stained with an early apoptosis indicator, annexin V, in conjunction with the vital dye propidium iodide. Annexin V binds to the negatively charged membrane phospholipid phosphatidylserine, which is translocated from the inner to the outer leaflet of the plasma membrane during the early stages of apoptosis, whereas propidium iodide binds to double-stranded nucleic acids and therefore probes the loss of membrane integrity in late apoptosis and/or necrosis. Accordingly, cells in early apoptosis should be annexin V positive and propidium iodide negative, whereas cells in late apoptosis or already dead should be both annexin V and propidium iodide positive. We found that mock-transfected cells were both annexin V and propidium iodide negative (Fig. 5A). In addition, a few APP_{WT}-transfected cells were annexin V positive, but no cells were propidium iodide positive. In contrast, abundant APP_{OSK}-transfected cells were annexin V positive; some APP_{OSK}-transfected cells were also propidium iodide positive, indicating late apoptosis.

To address the in vivo occurrence of Aβ oligomer-induced apoptosis, we examined expression of cleaved (i.e., activated) caspase-3 in the brains of 18-month-old APP_{OSK}-Tg mice by immunohistochemistry. Compared with the age-matched non-Tg littermates and APP_{WT}-Tg mice, the APP_{OSK}-Tg mice exhibited intense immunoreactivities to this activated form of caspase-3 in their hippocampi (Fig. 5B) and cerebral cortices (data not shown). We also examined the levels of cleaved caspase-3 in hippocampal homogenates of 18-month-old APP_{OSK}-Tg mice and non-Tg littermates. We detected increased levels of this activated form of caspase-3 in the Tg mice by Western blotting (Fig.

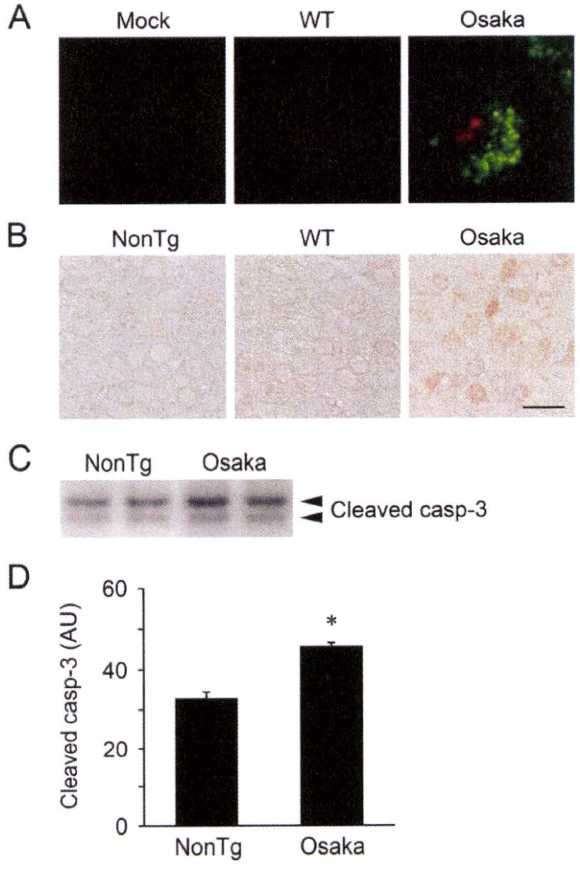

Fig. 5. Intracellular Aβ oligomers cause apoptosis. **A:** COS-7 cells mock transfected or transfected with APP_{WT} (WT) or APP_{OSK} (Osaka) were stained with an early apoptosis indicator, annexin V (green), in conjunction with the vital dye propidium iodide (red). Mock-transfected cells were negative for both annexin V and propidium iodide. A few APP_{WT}-transfected cells were annexin V positive cells, but there were no propidium iodide-positive cells. In contrast, more abundant APP_{OSK}-transfected cells were annexin V positive, and some of these cells were also propidium iodide positive, indicating late apoptosis. **B:** Brain sections of 18-month-old APP_{OSK}-Tg mice (Osaka), APP_{WT}-Tg mice (WT), and non-Tg littermates (NonTg) were stained with antibody to cleaved caspase-3. Compared with non-Tg littermates and APP_{WT}-Tg mice, the APP_{OSK}-Tg mice exhibited intense immunoreactivities to this activated form of caspase-3. The photographs show the hippocampal CA3 regions. **C,D:** Hippocampal homogenates with equal protein content of 18-month-old APP_{OSK}-Tg mice and non-Tg littermates were subjected to Western blotting for cleaved caspase-3 (casp-3). An increased level of cleaved caspase-3 was detected in APP_{OSK}-Tg mice. The figure shows representative blots. D: The signals of cleaved caspase-3 (both the upper and the lower bands) were quantified and expressed in arbitrary units (AU) per lane. Each result is presented as the mean ± SE (n = 4). $*P = 0.0003$ vs. non-Tg by unpaired Student's *t*-test. Scale bar = 20 μm.

5C,D). Thus, apoptosis was induced in vivo in association with intraneuronal accumulation of Aβ oligomers. Collectively, these results indicate that intraneuronal Aβ oligomers caused cell death by inducing ER stress, endosomal/lysosomal leakage, and mitochondrial dysfunction in vivo.

DISCUSSION

We previously demonstrated that the APP Osaka mutation induces the accumulation of Aβ oligomers in the ER and subsequent ER stress in COS-7 cells (Nishitsuji et al., 2009). ER stress elicits the UPR, which includes three responses that protect the cell against toxic buildup of misfolded proteins (Yoshida, 2007): 1) up-regulation of molecular chaperones to assist in protein refolding, 2) halt of further protein synthesis, and 3) ubiquitination of misfolded proteins and their translocation to proteasomes to degrade them (i.e., ERAD). We previously detected the first two responses in APP_{OSK}-transfected cells, i.e., enhanced induction of the molecular chaperone Grp78 and increased phosphorylation (i.e., inactivation) of the translation initiation factor eIF2α (Nishitsuji et al., 2009). In the present study, we demonstrated the occurrence of the last response, ERAD, by showing up-regulation of an E3 ubiquitin ligase, HRD1, in COS-7 cells. Consistent with these in vitro observations, we also observed accumulation of Aβ oligomers in ER and up-regulation of Grp78 and HRD1 in APP_{OSK}-Tg mouse brain. The occurrence of ERAD indicates that Aβ oligomers are transported from the ER into the cytoplasm, which may be a source of mitochondrial Aβ.

In addition to the ubiquitin-proteasome system, autophagy also participates in clearance of misfolded intracellular proteins. Autophagosomes engulf damaged organelles and aggregated proteins in the cytoplasm and sort them to lysosomes. The sorted materials are subsequently digested within autolysosomes that are formed by fusion of autophagosomes and lysosomes. Thus, the autophagy-lysosome system compensates for the deficiency of the ubiquitin-proteasome system, the latter of which is reportedly caused by excessive accumulation of intracellular Aβ (Almeida et al., 2006; Park et al., 2009). We previously reported that autophagy was markedly induced in APP_{OSK}-transfected cells (Nishitsuji et al., 2009). In spite of these protective mechanisms, severe and prolonged ER stress ultimately induces apoptosis. ER stress-induced apoptosis is mediated by activation of caspase-12 in rodents (Nakagawa et al., 2000) and caspase-4 in humans (Hitomi et al., 2004). We previously detected activation of both caspase-3 and −4 and DNA fragmentation in APP_{OSK}-transfected cells (Nishitsuji et al., 2009). Here we presented further evidence of apoptosis in APP_{OSK}-transfected cells using the annexin V and propidium iodide markers. In accordance with these in vitro observations, we revealed the occurrence of apoptosis in APP_{OSK}-Tg mice at 18 months of age with increased levels of activated caspase-3. These findings suggest that the APP Osaka mutation causes severe ER stress by producing Aβ oligomers beyond the capacity of UPR/autophagy cell survival systems. We supposed that the observed ER stress and apoptosis were attributed to intracellular accumulation of Aβ oligomers, rather than other APP-derived fragments such as soluble APP and the C-terminal fragments, because the control APP_{WT}-Tg mice displayed only slight increases in Grp78, HRD1, and activated caspase-3, despite the fact that they expressed human APP twice as much as APP_{OSK}-Tg mice (Tomiyama et al., 2010). Previously, we demonstrated that APP_{OSK}-Tg mice showed apparent neuronal loss in the hippocampus (particularly the CA3 region) at 24 months of age (Tomiyama et al., 2010). The present study showed the induction of apoptosis in several hippocampal and cortical neurons of APP_{OSK}-Tg mice at 18 months of age. As speculated previously, intracellular Aβ oligomer-induced neuronal death may require a long period of time in vivo and may occur in neurons vulnerable to Aβ oligomers.

Accumulation of Aβ oligomers was also observed in the endosomes/lysosomes of both APP_{OSK}-transfected cells and APP_{OSK}-Tg mouse brain. Exogenously applied Aβ has been shown to disrupt endosomal/lysosomal membrane impermeability and cause the leakage of the contents into the cytoplasm (Yang et al., 1998; Ditaranto et al., 2001; Ji et al., 2002). The acidic environment within endosomal/lysosomal vesicles accelerates Aβ aggregation, and the leakage likely occurs during this process. Aβ oligomers may assemble with one another to form pore-like structures in the membrane (Quist et al., 2005; Singer and Dewji, 2006; Kayed et al., 2009), and Aβ fibrils may grow during crossing of the membrane into the cytoplasm (Friedrich et al., 2010); both of these mechanisms should break down membrane impermeability. The present study demonstrated that endogenously generated Aβ oligomers induced endosomal/lysosomal leakage in both APP_{OSK}-transfected cells and APP_{OSK}-Tg mouse brain. Endosomal/lysosomal leakage is known to affect cellular functions profoundly and to cause cell death (Yang et al., 1998; D'Andrea et al., 2001; Ditaranto et al., 2001; Ji et al., 2002; Friedrich et al., 2010) and may be another source of mitochondrial Aβ. There are three possible origins or pathways of endosomal/lysosomal Aβ: 1) Aβ is secreted from cells by the secretary pathway and subsequently taken up from the extracellular space by endocytosis, 2) Aβ is generated within the endosomes by local processing of APP that is internalized from the plasma membrane via endocytosis, and 3) Aβ is transported from other intracellular compartments by the autophagic pathway. In the present study, we demonstrated that the first pathway contributed to endosomal/lysosomal leakage. Nevertheless, we conclude that the third pathway may also play a crucial role in endosomal/lysosomal leakage, because excessive accumulation of intraneuronal Aβ has been shown to cause both impairment of the autophagy-lysosome system (Yu et al., 2005; Ling et al., 2009) and eventually autolysosomal leakage that leads to cell death (Ling et al., 2009).

We found in the present study that Aβ oligomers also accumulated in mitochondria in both APP_{OSK}-transfected cells and APP_{OSK}-Tg mouse brain. Mitochondria are not typically thought to be a site of Aβ generation; it is assumed that mitochondrial Aβ is transported from other intracellular compartments (Hansson Petersen et al., 2008; Reddy, 2009). The potential origin of mitochondrial Aβ is possibly the ER and/or the endosomes/lysosomes, as mentioned above. However, it has been shown that both APP and γ-secretase components, including presenilin, nicastrin, Aph-1, and Pen-2, localize to mitochondria (Anandatheerthavarada et al., 2003; Hansson et al., 2004) and that APP has a mitochondrial targeting signal sequence (Anandatheerthavarada et al., 2003). These observations indicate the possibilities that at least a portion of mitochondrial Aβ is generated in situ and that Aβ may play a physiological, beneficial role for mitochondrial function. However, there is no evidence to date to confirm the physiological role of mitochondrial Aβ; instead, Aβ has been demonstrated to impair mitochondrial function (Keil et al., 2004; Caspersen et al., 2005; Crouch et al., 2005; Manczak et al., 2006; Eckert et al., 2008; Park et al., 2009; Yang et al., 2009; Yao et al., 2009). Interestingly, a portion of mitochondrial Aβ has been shown to form oligomers in AD, transgenic mouse brains and APP-transfected cells (Caspersen et al., 2005; Manczak et al., 2006). Furthermore, when it was applied exogenously, oligomeric and/or fibrillar Aβ, but not monomeric Aβ, displayed toxic effects (Crouch et al., 2005; Eckert et al., 2008; Yang et al., 2009). For APP_{OSK}-transfected cells, we demonstrated that mitochondrial accumulation of Aβ oligomers caused altered mitochondrial membrane potential and cytochrome c release from mitochondria. The latter was also observed in APP_{OSK}-Tg mouse brain. Aβ oligomer-induced mitochondrial dysfunction may be caused by the same mechanism at play in Aβ oligomer-induced endosomal/lysosomal leakage, whereby Aβ oligomers form pore-like structures in the membranes. Alternatively, Aβ may generate free radicals during aggregation and therefore cause oxidative damage to mitochondrial membranes and proteins. In either case, disruption of mitochondrial membrane impermeability allows passage of ions across the membranes and leads to their depolarization, the uncoupling of the respiratory chain from oxidative phosphorylation, and subsequently the release of cytochrome c. Injured mitochondria are also disposed by autophagy, which could overload the autophagy-lysosome system, resulting in enhanced lysosomal leakage.

It has been shown that there is cross-talk between cellular organelles (Ferri and Kroemer, 2001). In particular the ER and mitochondria are well known to interact via Ca^{2+} transfer and to regulate apoptosis (Pinton et al., 2008). Specifically, increased Ca^{2+} release from the ER causes excessive entry of this ion into mitochondria, which leads to apoptosis. Endosomal/lysosomal leakage has also been implicated in mitochondria-dependent apoptosis (Ferri and Kroemer, 2001). Both cathepsin D and a cathepsin-L-related protease released from late endosomes/lysosomes induce the proteolytic activation of Bid, a Bcl-2 family member, which generates a truncated Bid (t-Bid) that causes release of cytochrome c from mitochondria and activation of caspases-9 and −3 (Stoka et al., 2001; Heinrich et al., 2004). Thus, the enhanced release of cytochrome c from mitochondria in APP_{OSK}-transfected cells and in APP_{OSK}-Tg mouse brain may reflect, at least in part, both ER stress-induced Ca^{2+} release and lysosomal enzyme-mediated Bid activation (Fig. 6).

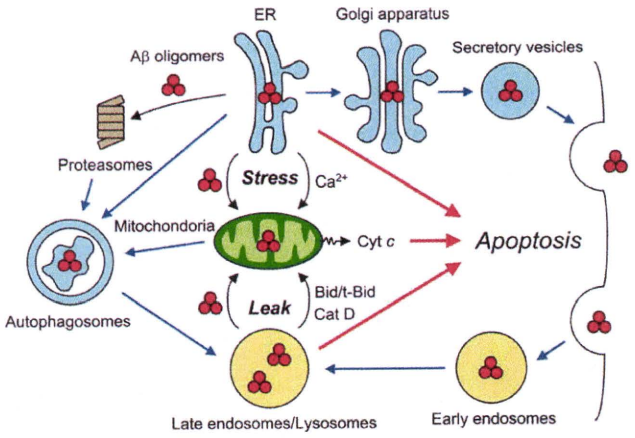

Fig. 6. Proposed mechanism underlying intracellular Aβ oligomer-induced cell death. Accumulation of Aβ oligomers in the ER causes ER stress that elicits the unfolded protein responses, including up-regulation of molecular chaperones, halt of further protein synthesis, and induction of ERAD. In ERAD, the Aβ oligomers are translocated from the ER into the cytoplasm to be degraded by proteasomes. Damaged ER and undegradable Aβ oligomers in the cytoplasm are engulfed by autophagosomes and sorted to lysosomes to be digested. In spite of these protective mechanisms, severe and prolonged ER stress activates caspase-4 in humans and initiates apoptosis. ER stress also induces Ca^{2+} release from the ER and causes excessive entry of Ca^{2+} into mitochondria, which elicits cytochrome c (Cyt c) release and apoptosis. Excessive formation of Aβ oligomers causes impairment of the autophagy-lysosome system, which results in disruption of endosomal/lysosomal membrane impermeability. Membrane disruption is also caused by Aβ taken up from the extracellular space by endocytosis and/or by Aβ generated within the endosomes via local processing of APP. Endosomal/lysosomal leakage profoundly affects cellular functions to cause cell death. Simultaneously, cathepsin D (Cat D) leaked from late endosomes/lysosomes activates Bid in the cytoplasm to generate t-Bid, which acts on mitochondria to induce cytochrome c release and apoptosis. A portion of Aβ oligomers in the cytoplasm, which presumably originate from the ER and endosomes/lysosomes, is sorted to mitochondria and directly damages their membranes, ultimately leading to apoptosis. Injured mitochondria are also disposed by autophagy, which may overload the autophagy-lysosome system, resulting in enhanced endosomal/lysosomal leakage. Thus, intracellular Aβ oligomers cause cell death by inducing ER stress, endosomal/lysosomal leakage, and mitochondrial dysfunction, both directly and indirectly.

Similar mechanisms have been proposed for mutant α-synuclein-induced cell death. It has been demonstrated

that expression of A53T-mutant α-synuclein in PC12 cells decreases proteasome activity, increases the reactive oxygen species level, and eventually causes cell death, which is accompanied by mitochondrial dysfunction (decreased membrane potential and increased cytochrome c release); ER stress (increased phosphorylated eIF2α and Grp78); and activation of caspases-12, −9, and −3 (Smith et al., 2005). In addition, it has been shown that proteosomal dysfunction in A53T-mutant α-synuclein-expressing cells is caused by α-synuclein oligomers (Emmanouilidou et al., 2010). Our finding in the present study that intracellular accumulation of peptide oligomers causes cell death by inducing ER stress, endosomal/lysosomal leakage, and mitochondrial dysfunction is not restricted to the APP Osaka mutation or AD but instead seems also to be plausible for other neurodegenerative disorders.

REFERENCES

Almeida CG, Takahashi RH, Gouras GK. 2006. β-amyloid accumulation impairs multivesicular body sorting by inhibiting the ubiquitin-proteasome system. J Neurosci 26:4277–4288.

Anandatheerthavarada HK, Biswas G, Robin MA, Avadhani NG. 2003. Mitochondrial targeting and a novel transmembrane arrest of Alzheimer's amyloid precursor protein impairs mitochondrial function in neuronal cells. J Cell Biol 161:41–54.

Caspersen C, Wang N, Yao J, Sosunov A, Chen X, Lustbader JW, Xu HW, Stern D, McKhann G, Yan SD. 2005. Mitochondrial Aβ: a potential focal point for neuronal metabolic dysfunction in Alzheimer's disease. FASEB J 19:2040–2041.

Crouch PJ, Blake R, Duce JA, Ciccotosto GD, Li QX, Barnham KJ, Curtain CC, Cherny RA, Cappai R, Dyrks T, Masters CL, Trounce IA. 2005. Copper-dependent inhibition of human cytochrome c oxidase by a dimeric conformer of amyloid-β1–42. J Neurosci 25:672–679.

D'Andrea MR, Nagele RG, Wang HY, Peterson PA, Lee DH. 2001. Evidence that neurones accumulating amyloid can undergo lysis to form amyloid plaques in Alzheimer's disease. Histopathology 38:120–134.

Ditaranto K, Tekirian TL, Yang AJ. 2001. Lysosomal membrane damage in soluble Aβ-mediated cell death in Alzheimer's disease. Neurobiol Dis 8:19–31.

Eckert A, Hauptmann S, Scherping I, Meinhardt J, Rhein V, Dröse S, Brandt U, Fändrich M, Müller WE, Götz J. 2008. Oligomeric and fibrillar species of β-amyloid (Aβ42) both impair mitochondrial function in P301L tau transgenic mice. J Mol Med 86:1255–1267.

Emmanouilidou E, Stefanis L, Vekrellis K. 2010. Cell-produced α-synuclein oligomers are targeted to, and impair, the 26S proteasome. Neurobiol Aging 31:953–968.

Fernández-Vizarra P, Fernández AP, Castro-Blanco S, Serrano J, Bentura ML, Martínez-Murillo R, Martínez A, Rodrigo J. 2004. Intra- and extracellular Aβ and PHF in clinically evaluated cases of Alzheimer's disease. Histol Histopathol 19:823–844.

Ferri KF, Kroemer G. 2001. Organelle-specific initiation of cell death pathways. Nat Cell Biol 3:E255–E263.

Friedrich RP, Tepper K, Rönicke R, Soom M, Westermann M, Reymann K, Kaether C, Fändrich M. 2010. Mechanism of amyloid plaque formation suggests an intracellular basis of Aβ pathogenicity. Proc Natl Acad Sci U S A 107:1942–1947.

Gouras GK, Tsai J, Naslund J, Vincent B, Edgar M, Checler F, Greenfield JP, Haroutunian V, Buxbaum JD, Xu H, Greengard P, Relkin NR. 2000. Intraneuronal Aβ42 accumulation in human brain. Am J Pathol 156:15–20.

Gouras GK, Tampellini D, Takahashi RH, Capetillo-Zarate E. 2010. Intraneuronal β-amyloid accumulation and synapse pathology in Alzheimer's disease. Acta Neuropathol 119:523–541.

Gyure KA, Durham R, Stewart WF, Smialek JE, Troncoso JC. 2001. Intraneuronal Aβ-amyloid precedes development of amyloid plaques in Down syndrome. Arch Pathol Lab Med 125:489–492.

Hansson CA, Frykman S, Farmery MR, Tjernberg LO, Nilsberth C, Pursglove SE, Ito A, Winblad B, Cowburn RF, Thyberg J, Ankarcrona M. 2004. Nicastrin, presenilin, APH-1, and PEN-2 form active γ-secretase complexes in mitochondria. J Biol Chem 279:51654–51660.

Hansson Petersen CA, Alikhani N, Behbahani H, Wiehager B, Pavlov PF, Alafuzoff I, Leinonen V, Ito A, Winblad B, Glaser E, Ankarcrona M. 2008. The amyloid β-peptide is imported into mitochondria via the TOM import machinery and localized to mitochondrial cristae. Proc Natl Acad Sci U S A 105:13145–13150.

Hashimoto M, Rockenstein E, Crews L, Masliah E. 2003. Role of protein aggregation in mitochondrial dysfunction and neurodegeneration in Alzheimer's and Parkinson's diseases. Neuromolecular Med 4:21–36.

Heinrich M, Neumeyer J, Jakob M, Hallas C, Tchikov V, Winoto-Morbach S, Wickel M, Schneider-Brachert W, Trauzold A, Hethke A, Schütze S. 2004. Cathepsin D links TNF-induced acid sphingomyelinase to Bid-mediated caspase-9 and −3 activation. Cell Death Differ 11:550–563.

Hitomi J, Katayama T, Eguchi Y, Kudo T, Taniguchi M, Koyama Y, Manabe T, Yamagishi S, Bando Y, Imaizumi K, Tsujimoto Y, Tohyama M. 2004. Involvement of caspase-4 in endoplasmic reticulum stress-induced apoptosis and Aβ-induced cell death. J Cell Biol 165:347–356.

Hoozemans JJ, Veerhuis R, Van Haastert ES, Rozemuller JM, Baas F, Eikelenboom P, Scheper W. 2005. The unfolded protein response is activated in Alzheimer's disease. Acta Neuropathol 110:165–172.

Hu X, Crick SL, Bu G, Frieden C, Pappu RV, Lee JM. 2009. Amyloid seeds formed by cellular uptake, concentration, and aggregation of the amyloid-β peptide. Proc Natl Acad Sci U S A 106:20324–20329.

Ji ZS, Miranda RD, Newhouse YM, Weisgraber KH, Huang Y, Mahley RW. 2002. Apolipoprotein E4 potentiates amyloid β peptide-induced lysosomal leakage and apoptosis in neuronal cells. J Biol Chem 277:21821–21828.

Kayed R, Pensalfini A, Margol L, Sokolov Y, Sarsoza F, Head E, Hall J, Glabe C. 2009. Annular protofibrils are a structurally and functionally distinct type of amyloid oligomer. J Biol Chem 284:4230–4237.

Keil U, Bonert A, Marques CA, Scherping I, Weyermann J, Strosznajder JB, Müller-Spahn F, Haass C, Czech C, Pradier L, Müller WE, Eckert A. 2004. Amyloid β-induced changes in nitric oxide production and mitochondrial activity lead to apoptosis. J Biol Chem 279:50310–50320.

Kikkert M, Doolman R, Dai M, Avner R, Hassink G, van Voorden S, Thanedar S, Roitelman J, Chau V, Wiertz E. 2004. Human HRD1 is an E3 ubiquitin ligase involved in degradation of proteins from the endoplasmic reticulum. J Biol Chem 279:3525–3534.

Klein WL, Krafft GA, Finch CE. 2001. Targeting small Aβ oligomers: the solution to an Alzheimer's disease conundrum? Trends Neurosci 24:219–224.

LaFerla FM, Green KN, Oddo S. 2007. Intracellular amyloid-β in Alzheimer's disease. Nat Rev Neurosci 8:499–509.

Lambert MP, Velasco PT, Chang L, Viola KL, Fernandez S, Lacor PN, Khuon D, Gong Y, Bigio EH, Shaw P, De Felice FG, Krafft GA, Klein WL. 2007. Monoclonal antibodies that target pathological assemblies of Aβ. J Neurochem 100:23–35.

Ling D, Song HJ, Garza D, Neufeld TP, Salvaterra PM. 2009. Aβ42-induced neurodegeneration via an age-dependent autophagic-lysosomal injury in *Drosophila*. PLoS One 4:e4201.

Manczak M, Anekonda TS, Henson E, Park BS, Quinn J, Reddy PH. 2006. Mitochondria are a direct site of Aβ accumulation in Alzheimer's disease neurons: implications for free radical generation and oxidative damage in disease progression. Hum Mol Genet 15:1437–1449.

Matsuyama S, Teraoka R, Mori H, Tomiyama T. 2007. Inverse correlation between amyloid precursor protein and synaptic plasticity in transgenic mice. Neuroreport 18:1083–1087.

Mori C, Spooner ET, Wisniewsk KE, Wisniewski TM, Yamaguch H, Saido TC, Tolan DR, Selkoe DJ, Lemere CA. 2002. Intraneuronal Aβ42 accumulation in Down syndrome brain. Amyloid 9:88–102.

Nakagawa T, Zhu H, Morishima N, Li E, Xu J, Yankner BA, Yuan J. 2000. Caspase-12 mediates endoplasmic-reticulum-specific apoptosis and cytotoxicity by amyloid-β. Nature 403:98–103.

Nishitsuji K, Tomiyama T, Ishibashi K, Ito K, Teraoka R, Lambert MP, Klein WL, Mori H. 2009. The E693Δ mutation in amyloid precursor protein increases intracellular accumulation of amyloid β oligomers and causes endoplasmic reticulum stress-induced apoptosis in cultured cells. Am J Pathol 174:957–969.

Park HJ, Kim SS, Kang S, Rhim H. 2009. Intracellular Aβ and C99 aggregates induce mitochondria-dependent cell death in human neuroglioma H4 cells through recruitment of the 20S proteasome subunits. Brain Res 1273:1–8.

Pinton P, Giorgi C, Siviero R, Zecchini E, Rizzuto R. 2008. Calcium and apoptosis: ER-mitochondria Ca^{2+} transfer in the control of apoptosis. Oncogene 27:6407–6418.

Quist A, Doudevski I, Lin H, Azimova R, Ng D, Frangione B, Kagan B, Ghiso J, Lal R. 2005. Amyloid ion channels: a common structural link for protein-misfolding disease. Proc Natl Acad Sci U S A 102:10427–10432.

Reddy PH. 2009. Amyloid β, mitochondrial structural and functional dynamics in Alzheimer's disease. Exp Neurol 218:286–292.

Selkoe DJ. 2002. Alzheimer's disease is a synaptic failure. Science 298:789–791.

Singer SJ, Dewji NN. 2006. Evidence that Perutz's double-β-stranded subunit structure for β-amyloids also applies to their channel-forming structures in membranes. Proc Natl Acad Sci U S A 103:1546–1550.

Smith WW, Jiang H, Pei Z, Tanaka Y, Morita H, Sawa A, Dawson VL, Dawson TM, Ross CA. 2005. Endoplasmic reticulum stress and mitochondrial cell death pathways mediate A53T mutant α-synuclein-induced toxicity. Hum Mol Genet 14:3801–3811.

Stoka V, Turk B, Schendel SL, Kim TH, Cirman T, Snipas SJ, Ellerby LM, Bredesen D, Freeze H, Abrahamson M, Bromme D, Krajewski S, Reed JC, Yin XM, Turk V, Salvesen GS. 2001. Lysosomal protease pathways to apoptosis. Cleavage of bid, not pro-caspases, is the most likely route. J Biol Chem 276:3149–3157.

Suga K, Tomiyama T, Mori H, Akagawa K. 2004. Syntaxin 5 interacts with presenilin holoproteins, but not with their N- or C-terminal fragments, and affects β-amyloid peptide production. Biochem J 381:619–628.

Takahashi RH, Milner TA, Li F, Nam EE, Edgar MA, Yamaguchi H, Beal MF, Xu H, Greengard P, Gouras GK. 2002. Intraneuronal Alzheimer Aβ42 accumulates in multivesicular bodies and is associated with synaptic pathology. Am J Pathol 161:1869–1879.

Takahashi RH, Almeida CG, Kearney PF, Yu F, Lin MT, Milner TA, Gouras GK. 2004. Oligomerization of Alzheimer's β-amyloid within processes and synapses of cultured neurons and brain. J Neurosci 24:3592–3599.

Tomiyama T, Nagata T, Shimada H, Teraoka R, Fukushima A, Kanemitsu H, Takuma H, Kuwano R, Imagawa M, Ataka S, Wada Y, Yoshioka E, Nishizaki T, Watanabe Y, Mori H. 2008. A new amyloid β variant favoring oligomerization in Alzheimer's-type dementia. Ann Neurol 63:377–387.

Tomiyama T, Matsuyama S, Iso H, Umeda T, Takuma H, Ohnishi K, Ishibashi K, Teraoka R, Sakama N, Yamashita T, Nishitsuji K, Ito K, Shimada H, Lambert MP, Klein WL, Mori H. 2010. A mouse model of amyloid β oligomers: their contribution to synaptic alteration, abnormal tau phosphorylation, glial activation, and neuronal loss in vivo. J Neurosci 30:4845–4856.

Wirths O, Multhaup G, Bayer TA. 2004. A modified β-amyloid hypothesis: intraneuronal accumulation of the β-amyloid peptide—the first step of a fatal cascade. J Neurochem 91:513–520.

Yang AJ, Chandswangbhuvana D, Margol L, Glabe CG. 1998. Loss of endosomal/lysosomal membrane impermeability is an early event in amyloid Aβ1–42 pathogenesis. J Neurosci Res 52:691–698.

Yang TT, Hsu CT, Kuo YM. 2009. Cell-derived soluble oligomers of human amyloid-β peptides disturb cellular homeostasis and induce apoptosis in primary hippocampal neurons. J Neural Transm 116:1561–1569.

Yao J, Irwin RW, Zhao L, Nilsen J, Hamilton RT, Brinton RD. 2009. Mitochondrial bioenergetic deficit precedes Alzheimer's pathology in female mouse model of Alzheimer's disease. Proc Natl Acad Sci U S A 106:14670–14675.

Yoshida H. 2007. ER stress and diseases. FEBS J 274:630–658.

Yu WH, Cuervo AM, Kumar A, Peterhoff CM, Schmidt SD, Lee JH, Mohan PS, Mercken M, Farmery MR, Tjernberg LO, Jiang Y, Duff K, Uchiyama Y, Näslund J, Mathews PM, Cataldo AM, Nixon RA. 2005. Macroautophagy—a novel β-amyloid peptide-generating pathway activated in Alzheimer's disease. J Cell Biol 171:87–98.